MITSUBISHI ELECTRIC RESEARCH LABORATORIES
https://www.merl.com

Analytical reformulation of LMTD and effectiveness-NTU methods for two-phase heat transfer with pressure drop and temperature glide

Qiao, Hongtao

TR2026-103 July 03, 2026

Abstract

This work addresses the challenge of accurately modeling heat transfer in two-phase heat exchangers using zeotropic refrigerants, where conventional methods often fail due to the omission of pressure drop and temperature glide effects. To overcome these limitations, we present modified formulations of the Log Mean Temperature Difference (LMTD) and effectiveness–NTU methods, introducing dimensionless correction parameters that quantify glide intensity and pressure-induced saturation temperature variation. Closed-form solutions are developed for parallel-flow, counterflow, and cross-flow configurations. Comparative analysis shows that the classical LMTD method can overestimate heat transfer by more than 10% in counter flow and underestimate it by a similar margin in parallel flow under strong glide and pressure drop. The modified effectiveness–NTU approach offers even greater improvements, with corrections up to 40%, depending on glide magnitude and heat capacity ratio. In cross-flow systems, the combined influence of glide and pressure drop causes non-monotonic deviations reaching 30% under high-glide, high-pressuredrop conditions. A curvature-based evaluation of temperature profiles offers additional insight into the thermodynamic asymmetries that distort classical predictions. The proposed framework applies to both single- and two-phase regimes, providing a unified, accurate, and analytically tractable tool for heat exchanger design and thermal performance evaluation under realistic conditions.

International Journal of Heat and Mass Transfer 2025

Mitsubishi Electric Research Laboratories, Inc.
201 Broadway, Cambridge, Massachusetts 02139

Analytical reformulation of LMTD and effectiveness-NTU methods for two-phase heat transfer with pressure drop and temperature glide

Hongtao Qiao*

Mitsubishi Electric Research Laboratories, 201 Broadway, Cambridge, MA 02139, USA

*: Corresponding Author, Tel: +1 (617) 621-7586, E-mail: qiao@merl.com

ABSTRACT

This work addresses the challenge of accurately modeling heat transfer in two-phase heat exchangers using zeotropic refrigerants, where conventional methods often fail due to the omission of pressure drop and temperature glide effects. To overcome these limitations, we present modified formulations of the Log Mean Temperature Difference (LMTD) and effectiveness–NTU methods, introducing dimensionless correction parameters that quantify glide intensity and pressure-induced saturation temperature variation. Closed-form solutions are developed for parallel-flow, counter-flow, and cross-flow configurations. Comparative analysis shows that the classical LMTD method can overestimate heat transfer by more than 10% in counter flow and underestimate it by a similar margin in parallel flow under strong glide and pressure drop. The modified effectiveness–NTU approach offers even greater improvements, with corrections up to 40%, depending on glide magnitude and heat capacity ratio. In cross-flow systems, the combined influence of glide and pressure drop causes non-monotonic deviations reaching 30% under high-glide, high-pressure-drop conditions. A curvature-based evaluation of temperature profiles offers additional insight into the thermodynamic asymmetries that distort classical predictions. The proposed framework applies to both single- and two-phase regimes, providing a unified, accurate, and analytically tractable tool for heat exchanger design and thermal performance evaluation under realistic conditions.

Keywords: LMTD method; Effectiveness-NTU method; Pressure drop; Temperature glide; Two-phase heat transfer; Zeotropic mixtures

NOMENCLATURE

A	area [m^2]
C	capacitance [W/K]
c_p	specific heat [J/(kg K)]
h	specific enthalpy [J/kg]
$\dot{m}$	mass flow rate [kg/s]
NTU	number of transfer units [-]
p	pressure [Pa]
Q	heat transfer rate [W]
T	temperature [K]
U	overall heat transfer coefficient [W/(m^2 K)]
δ	difference [-]
ε	effectiveness [-]
ϕ	capacitance ratio [-]
γ	normalized saturation temperature shift [-]

Subscripts

bub	bubble point
cl	classical method
dev	deviation
dew	dew point

f	fluid
g	temperature glide related
HX	heat exchanger
in	inlet
m	mean
mod	modified method
out	outlet
p	pressure related
r	refrigerant
sat	saturation
SP	single-phase
TP	two-phase

1. Introduction

Heat exchangers are critical components in a wide range of thermal systems, including refrigeration, air-conditioning, power generation, chemical processing, and energy storage. Accurate modeling of their thermal performance is essential for effective system design and optimization. Among the available modeling approaches, the Log Mean Temperature Difference (LMTD) and effectiveness–NTU (ε–NTU) methods are widely adopted due to their analytical simplicity, closed-form nature, and historical reliability [1].

However, both methods rely on several idealized assumptions, including constant fluid properties, negligible pressure drop, and isothermal phase change. These assumptions are frequently violated in real-world applications involving zeotropic refrigerant mixtures, which undergo temperature glide during phase change and often experience non-negligible pressure drop along the flow path. Temperature glide leads to variation in the saturation temperature with vapor quality even under constant pressure, while pressure drop further shifts the saturation point, causing refrigerant temperature to vary along the flow direction. Consequently, the actual thermal behavior departs significantly from the constant-temperature phase change assumptions inherent to classical models.

When pressure drop and temperature glide are neglected, the LMTD and ε–NTU methods can yield substantial errors in heat exchanger performance prediction—often underestimating or overestimating the mean temperature difference and overall effectiveness. This issue was identified early by Itard and Machielsen [2], who concluded that the classical LMTD method is inadequate for systems involving significant pressure drop and temperature glide, such as compression/resorption heat pumps using zeotropic refrigerants. Lundqvist [3] briefly acknowledged the limitations of LMTD but focused primarily on differences among subcooled,

condensing, and superheating regimes, without addressing the nonlinearities present in the two-phase region. Schaefer and Shelton [4] further emphasized that the unique thermodynamic behavior of zeotropic mixtures has a profound impact on the design and operation of vapor compression systems, highlighting the need for modeling approaches that explicitly account for glide and composition-dependent effects. Rajapaksha [5] extended this analysis by evaluating the accuracy of LMTD calculations for refrigerant mixtures and demonstrated that deviations from ideal behavior, particularly under two-phase flow, can result in significant discrepancies in predicted heat transfer performance.

Despite these recognized limitations, no unified, closed-form model currently exists that simultaneously incorporates both temperature glide and pressure-drop-induced saturation temperature shifts within the standard LMTD or ε–NTU frameworks across common heat exchanger configurations. This absence of a generalized analytical formulation represents a critical gap in existing heat exchanger theory and limits the predictive accuracy of current design methods for systems involving zeotropic refrigerants.

Several studies have attempted to relax some of the restrictive assumptions in the classical LMTD method, but these efforts have generally focused on separate or peripheral issues. Wong et al. [6] proposed a "log mean heat transfer rate" method that incorporates radiative heat transfer under low-convection conditions. Cui et al. [7] developed a modified LMTD framework for indirect evaporative heat exchangers where latent heat plays a dominant role. Claesson [8] introduced a correction based on heat-flux-dependent boiling for compact brazed plate evaporators. Utamura et al. [9] generalized the LMTD method to accommodate varying fluid properties under supercritical conditions. Mistry and Misener [10] applied convexity theory to optimize heat exchanger networks using the LMTD function.

Parallel developments have extended the ε–NTU framework to specialized systems. Nellis and Pfotenhauer [11] incorporated external heat transfer into the ε–NTU formulation for counterflow exchangers. Alquaity et al. [12] examined the impact of kinetic energy variation and external heat leaks in parallel-flow exchangers. Ren [13, 14] proposed corrections for packed bed cooling towers and desiccant systems using single- and double-film models. Other application-specific extensions include NTU models for membrane dehumidification [15], latent thermal storage [16], cooling/dehumidifying coils with non-unity Lewis factor [17], humidifiers [18], and air-cooled heat exchangers [19].

Although these efforts have successfully extended classical models to a broader set of applications and boundary conditions, none have directly addressed the coupled effects of pressure drop and temperature glide in two-phase flows of zeotropic refrigerants. This is a critical omission, as such effects often occur simultaneously in practical systems and introduce strongly interacting influences on the thermal driving force. Furthermore, most previous extensions are either limited to specific geometries, rely on empirical or numerical corrections, or sacrifice analytical clarity, reducing their generality and utility for design.

To bridge this gap, the present work develops a unified, closed-form analytical reformulation of both the LMTD and ε–NTU methods that explicitly incorporates both refrigerant pressure drop and temperature glide. The proposed framework is broadly applicable to parallel-, counter-, and cross-flow configurations and remains valid in both single- and two-phase flow regimes, making it practical for a wide range of engineering applications.

The key contributions and novelty of this work are:

- A unified analytical framework that extends and corrects the classical LMTD and ε–NTU methods by incorporating temperature glide and pressure drop effects in two-phase zeotropic refrigerant flows;
- Closed-form expressions for key performance quantities using correction factors tied to physical parameters;
- A curvature-based interpretation of temperature profiles that provides physical insight into model error and local temperature behavior;
- Error mapping that delineates the range of validity of classical models and quantifies the benefit of correction;
- Identification of limiting cases where classical methods remain accurate and explicit criteria for when correction becomes necessary.

The remainder of the paper is organized as follows. Section 2 presents the derivation of the corrected LMTD method. Section 3 develops the modified ε–NTU relations. Section 4 provides detailed error analysis and discussions of curvature and temperature profiles across different configurations. Section 5 summarizes the key findings and implications of the study.

2. Modified LMTD approach

The LMTD method is a classical tool used to evaluate the total heat transfer in a heat exchanger. It relates the heat transfer rate to the overall heat transfer coefficient, the total heat transfer area, and the temperature difference between the two fluids at each end of the exchanger. This method is particularly effective when the inlet and outlet temperatures of both fluids are known, and the temperature profiles vary logarithmically along the flow direction.

The classical LMTD expression, typically derived under steady-state and idealized assumptions, is given by

$$Q = U \cdot A \cdot LMTD \tag{1}$$

$$LMTD = \frac{\Delta T_1 - \Delta T_2}{\ln\left(\Delta T_1 / \Delta T_2\right)} \tag{2}$$

where ΔT_1 and ΔT_2 are the temperature differences between the two fluids at each end of the heat exchanger, U is the overall heat transfer coefficient and A is the taoheat transfer area.

The derivation of this classical formulation is well established and can be found in standard heat transfer texts and is therefore not repeated here. However, the key assumptions underlying its applicability are briefly summarized as follows: (1) no heat loss to the surroundings, i.e., heat transfer occurs exclusively between the hot and cold fluids; (2) steady-state flow conditions; (3) negligible axial conduction; (4) negligible changes in potential and kinetic energy; (5) constant specific heats for fluids not undergoing phase change; and (6) a uniform overall heat transfer coefficient throughout the heat exchanger.

A critical but often overlooked assumption is that fluid temperature variations—especially in the phase-change stream—are driven solely by heat exchange. This assumption breaks down in systems using zeotropic refrigerants or experiencing appreciable pressure drop, where temperature variations also arise from thermodynamic properties and flow-induced pressure changes.

Fig. 1 illustrates a realistic phase change process of a zeotropic refrigerant mixture, progressing from point 1 to point 2 within the two-phase region. The saturation envelope, bounded by the bubble point and dew point curves, demonstrates temperature glide at constant pressure due to the mixture's zeotropic nature. Additionally, the downward slope from point 1 to point 2 captures the effect of pressure drop along the flow path, which reduces both the bubble and dew point temperatures. This combined effect leads to a sloped, non-isothermal phase-change trajectory during condensation or evaporation—markedly different from the constant-temperature assumption in classical models.

Consequently, applying the conventional LMTD method to such systems can yield substantial errors in predicted heat transfer. To address these limitations, the following sections develop a modified LMTD formulation that explicitly accounts for pressure drop and temperature glide in two-phase flows. This generalized approach improves predictive accuracy for the analysis and design of heat exchangers operating with zeotropic refrigerants under non-ideal conditions.

2.1 Parallel-flow and counter-flow configurations

To illustrate the derivation, we first consider two fundamental configurations: a parallel-flow heat exchanger and a counter-flow heat exchanger, shown in Fig. 2 and Fig. 3, respectively. These configurations provide a representative framework for analyzing the thermal behavior under two-phase conditions. In both cases, the hot stream is a condensing zeotropic refrigerant, and the cold stream is a single-phase secondary fluid, such as air or brine. The derivations presented here are equally applicable to evaporation scenarios.

Due to the zeotropic nature of the refrigerant, its temperature decreases progressively along the heat exchanger, influenced by both temperature glide—a result of changing composition during phase change—and pressure drop—which lowers the local saturation temperature. To simplify the analysis while capturing the dominant effects, the following assumptions are made:

1. The refrigerant temperature change during phase change is attributed to both pressure variation and temperature glide.
2. The temperature change due to glide varies linearly in two-phase.
3. The temperature change due to pressure loss is assumed to vary linearly along the flow path and is approximated by the average change in dew point and bubble point temperatures, representing the overall shift in saturation temperature induced by pressure variation.

In the ideal case of phase change at constant pressure and temperature, the specific heat of the refrigerant is effectively infinite. However, in the presence of glide, a mean pseudo two-phase specific heat can be defined to account for the finite temperature change over a isobaric phase transition

$$c_{p,TP} = \frac{h_{dew} - h_{bub}}{T_{dew} - T_{bub}} \tag{3}$$

where the subscripts "dew" and "bub" denote the dew point and bubble point, respectively. Correspondingly, the thermal capacitance rates of the refrigerant and the fluid can be defined as $C_r = \dot{m}_r c_{p,TP}$ and $C_f = \dot{m}_f c_{p,f}$, respectively.

Since the refrigerant temperature depends on both pressure and enthalpy, it can be generally expressed as a function $T = T(p,h)$. Thus, the total differential of temperature is

$$dT = \left(\frac{\partial T}{\partial p}\right)_h dp + \left(\frac{\partial T}{\partial h}\right)_p dh \tag{4}$$

Within the two-phase region, the saturation temperature of a zeotropic refrigerant changes gradually with enthalpy at constant pressure due to temperature glide. The partial derivative $(\partial T/\partial h)_p$ quantifies the rate of temperature change with respect to specific enthalpy and is the inverse of $(\partial h/\partial T)_p$, which is analogous to the definition of specific heat capacity. Although true specific heat is not defined in the two-phase region, it is reasonable to assume that this derivative remains approximately constant over the glide range at a fixed pressure. Therefore, we approximate $(\partial h/\partial T)_p$ using the reciprocal of a pseudo two-phase specific heat, as defined in Eq. (3), to capture the average thermodynamic behavior of the mixture during phase change, i.e.,

$$\left(\frac{\partial T}{\partial h}\right)_p = \left(\frac{\partial h}{\partial T}\right)_p^{-1} \approx \frac{T_{dew} - T_{bub}}{h_{dew} - T_{bub}} = \frac{1}{c_{p,TP}} \tag{5}$$

In zeotropic refrigerant mixtures, the saturation temperature is pressure-dependent, meaning that both the dew point and bubble point temperatures shift as pressure changes. This effect is especially important in two-phase flow where pressure drop along the heat exchanger length is non-negligible. The partial derivative $(\partial T/\partial p)_h$ quantifies local sensitivity of temperature to pressure at constant enthalpy. In general, $(\partial T/\partial p)_h$ is difficult to evaluate directly due to the nonlinear nature of two-phase thermodynamic properties. However, it can be reasonably approximated by averaging the slopes of the dew point and bubble point temperature curves with respect to pressure. This approach provides a practical and bounded estimate with minimal error. For example, at 1 MPa for R-454C, the average of $\mathrm{d}T_{dew}/\mathrm{d}p$ and $\mathrm{d}T_{bub}/\mathrm{d}p$ is approximately 3.59×10^{-5} K/Pa. Across the entire two-phase region, the variation in $(\partial T/\partial p)_h$ remains within 3% of this average value, confirming the accuracy and robustness of the approximation. To express this derivative in terms of measurable inlet and outlet conditions, we apply a finite difference approximation across the heat exchanger. This allows us to represent the partial derivative using an average condition that captures the overall thermodynamic behavior, while significantly simplifying the analytical formulation.

$$\left(\frac{\partial T}{\partial p}\right)_h \approx \frac{1}{2}\left(\frac{dT_{dew}}{dp}+\frac{dT_{bub}}{dp}\right) \approx \frac{\Delta T_{dew}+\Delta T_{bub}}{2\Delta p_{HX}} = \frac{\Delta T_{sat}}{\Delta p_{HX}} \tag{6}$$

where Δp_{HX} is the pressure change across the heat exchanger, and ΔT_{dew} and ΔT_{bub} are the changes in dew point and bubble point temperatures, respectively. These are defined as $\Delta T_{dew} = T_{dew,out} - T_{dew,in}$, $\Delta T_{bub} = T_{bub,out} - T_{bub,in}$, $\Delta T_{sat} = (\Delta T_{dew} + \Delta T_{bub})/2$. This simplification significantly facilitates analytical modeling without introducing appreciable error in the calculation of temperature gradients within two-phase flow regions.

Combining these contributions, the refrigerant temperature can be expressed as the sum of glide- and pressure-induced components

$$T_r = T_{r,in} + \Delta T_p + \Delta T_g \tag{7}$$

where ΔT_p and ΔT_g represent the temperature changes due to pressure drop and temperature glide, respectively. Substituting Eqs. (5) and (6) into Eq. (7), we obtain

$$T_r = T_{r,in} + \frac{\Delta p}{\Delta p_{HX}} \Delta T_{sat} + \frac{\dot{m}_r \left(h_r - h_{r,in} \right)}{C_r} \tag{8}$$

Assuming the pressure drop is linearly proportional to the flow length, we model the spatial dependence of pressure drop as

$$\Delta p / \Delta p_{HX} \approx L / L_{HX} = A / A_{HX} \tag{9}$$

where A_{HX} is the total heat exchanger area.

To quantify the energy exchange, we define the heat transfer rate from the inlet (at area $A = 0$) to a general location A (a positive heat transfer rate indicates energy transfer from the refrigerant to the secondary fluid, while a negative value corresponds to heat transfer in the opposite direction)

$$Q = \dot{m}_r \left(h_{r,in} - h_r \right) \tag{10}$$

Substituting into Eq. (8) and rearranging terms yields the following expression for the local refrigerant temperature profile

$$T_r = T_{r,in} + \frac{A}{A_{HX}} \Delta T_{sat} - \frac{Q}{C_r} \tag{11}$$

Assuming single-phase flow with constant specific heat, the temperature of the secondary fluid varies along the heat exchanger and depends on the flow configuration—parallel or counter-flow—as illustrated in Fig. 2 and Fig. 3. This temperature distribution can be expressed as

$$T_f = \begin{cases} T_{f,in} + Q/C_f & \text{for parallel flow} \\ T_{f,out} - Q/C_f & \text{for counter flow} \end{cases} \tag{12}$$

The differential temperature changes of the refrigerant and the fluid are given by

$$dT_r = \frac{\Delta T_{sat}}{A_{HX}} dA - \frac{1}{C_r} dQ \tag{13}$$

$$dT_f = \pm \frac{1}{C_f} dQ \tag{14}$$

where the upper and lower signs correspond to the parallel-flow and counter-flow configurations, respectively.

Subtracting Eq. (14) from Eq. (13) yields the following differential equation for the local temperature difference between the refrigerant and the fluid

$$d(\Delta T) = -\frac{1}{C_f}(\phi \pm 1) dq + \frac{\Delta T_{sat}}{A_{HX}} dA \tag{15}$$

Here, $\Delta T = T_r - T_f$, and the capacitance ratio $\phi = \frac{C_f}{C_r}$.

The heat transfer rate across a differential area dA can be expressed using the local temperature difference

$$dQ = U \Delta T dA \tag{16}$$

Substituting Eq. (16) into Eq. (15) and rearranging terms leads to

$$\frac{d\Delta T}{-\frac{1}{C_f}(\phi \pm 1) U \Delta T + \frac{\Delta T_{sat}}{A_{HX}}} = dA \tag{17}$$

Letting $\alpha = -(\phi \pm 1)U/C_f$ and $\beta = \Delta T_{sat}/A_{HX}$, and integrating both sides of Eq. (17), we obtain

$$\Delta T = \left(\Delta T_1 + \frac{\beta}{\alpha} \right) \exp(\alpha A) - \frac{\beta}{\alpha} \tag{18}$$

where $\frac{\beta}{\alpha} = -\frac{\Delta T_{sat}}{(\phi \pm 1)\,\mathrm{NTU}}$, defined by introducing the number of transfer units $\mathrm{NTU} = \frac{UA_{HX}}{C_f}$.

Eq. (18) gives the local temperature difference between the refrigerant and the fluid at any point along the heat exchanger. To determine the overall mean temperature difference, we define

$$\Delta T_m = \frac{1}{A_{HX}} \int_0^{A_{HX}} \Delta T dA \tag{19}$$

Substituting Eq. (18) into Eq. (19) and integrating over the full area yields

$$\Delta T_m = \frac{1}{\alpha A_{HX}} \left(\Delta T_1 + \frac{\beta}{\alpha} \right) \left(\exp(\alpha A_{HX}) - 1 \right) - \frac{\beta}{\alpha} \tag{20}$$

According to Eq. (18), the temperature difference between refrigerant and fluid at the outlet (point 2) is

$$\Delta T_2 = (\Delta T_1 + \beta / \alpha) \exp(\alpha A_{HX}) - \beta / \alpha \tag{21}$$

This allows us to express the ratio of the terminal temperature differences as

$$\alpha A_{HX} = \ln\left((\Delta T_2 + \beta / \alpha) / (\Delta T_1 + \beta / \alpha) \right) \tag{22}$$

Substituting Eq. (22) into Eq. (20) leads to the final expression for the corrected LMTD

$$LMTD = \frac{\Delta T_2 - \Delta T_1}{\ln\left(\left(\Delta T_2 + \frac{\beta}{\alpha} \right) / \left(\Delta T_1 + \frac{\beta}{\alpha} \right) \right)} - \frac{\beta}{\alpha} \tag{23}$$

The modified LMTD formulation introduces two key parameters—α and β—which quantify the effects of temperature glide and pressure drop in the two-phase refrigerant, respectively:

- α reflects how temperature glide changes the spatial variation of the refrigerant temperature, affecting the shape of the temperature difference curve along the exchanger.

- β quantifies the saturation temperature gradient along the heat exchanger length due to refrigerant-side pressure drop. A nonzero β shifts the refrigerant temperature profile downward, influencing the local temperature difference and thus the LMTD.

The term β/α represents the normalized influence of pressure drop relative to the curvature induced by temperature glide. This ratio governs both the shape and magnitude of the effective mean temperature difference, and it plays a central role in modifying the classical LMTD to more accurately represent the thermodynamic behavior of two-phase flow with zeotropic refrigerants. By incorporating β/α into Eq. (23), the combined effects of pressure drop and temperature glide are analytically embedded into the corrected LMTD formulation, i.e.,

$$LMTD^{\text{parallel/counter}} = \frac{\Delta T_2 - \Delta T_1}{\ln\left(\left(\Delta T_2 - \frac{\Delta T_{sat}}{(\phi \pm 1)\,\text{NTU}}\right) \Big/ \left(\Delta T_1 - \frac{\Delta T_{sat}}{(\phi \pm 1)\,\text{NTU}}\right)\right)} + \frac{\Delta T_{sat}}{(\phi \pm 1)\,\text{NTU}} \tag{24}$$

where the upper and lower signs apply to the parallel-flow and counter-flow configurations, respectively. For the parallel-flow case, the terminal temperature differences are defined as $\Delta T_1 = T_{\text{r,in}} - T_{\text{f,in}}$ and $\Delta T_2 = T_{\text{r,out}} - T_{\text{f,out}}$; For counter-flow, they are $\Delta T_1 = T_{\text{r,in}} - T_{\text{f,out}}$ and $\Delta T_2 = T_{\text{r,out}} - T_{\text{f,in}}$.

In general, the ratio β/α is positive for parallel-flow and negative for counter-flow configurations. Eq. (24) is valid for both condensation and evaporation processes. In condensation, the mean temperature difference is positive, while in evaporation it is negative (since both ΔT_1 and ΔT_2 are typically negative). When the refrigerant (either a pure substance or azeotropic mixture) exhibits negligible temperature glide, the corrected LMTD simplifies by taking $\phi = 0$ (reflecting $C_r \to \infty$). Further, when refrigerant pressure drop is negligible ($\Delta T_{\text{sat}} = 0$), Eq. (24) collapses to the classical LMTD formula, thereby validating the consistency of the generalized expression.

2.2 Crossflow configuration with mixed refrigerant and unmixed secondary fluid

Building upon the modified formulations developed for parallel-flow and counter-flow configurations, we now extend the analysis to the cross-flow configuration, which is prevalent in compact heat exchangers such as microchannel and fin-and-tube designs. These geometries are widely used in HVAC and refrigeration systems due to their high heat transfer surface area density and efficient thermal performance.

In the configuration under consideration, a zeotropic refrigerant flows inside straight circular or microchannel tubes, while a single-phase secondary fluid flows perpendicularly across the outer surface of the tubes, typically through fin passages. This arrangement is representative of tube-fin heat exchangers, where the refrigerant is assumed to be fully mixed in the transverse direction, leading to a temperature field that depends solely on the longitudinal coordinate. In contrast, the secondary fluid is considered unmixed, such that its temperature varies in both the streamwise and transverse directions. This mixed–unmixed configuration leads to a spatially non-uniform temperature difference between the two streams. The analysis becomes more complex when refrigerant pressure drop and temperature glide are considered, as these effects introduce coupling between local enthalpy variation and temperature difference along the flow path. Under such conditions, a generalized LMTD formulation is required to accurately characterize the heat transfer behavior.

Fig. 4 illustrates the cross-flow domain analyzed in this study. The refrigerant flows along the x-direction inside a single tube and is assumed to be fully mixed, resulting in a temperature field $T_r(x)$ that varies only with the longitudinal coordinate. In contrast, the secondary fluid flows in the transverse y-direction and is considered unmixed, leading to a two-dimensional temperature distribution $T_f(x,y)$. Two differential control volumes are identified in the schematic, (1) a shaded patch of area $dxdy$, used to derive the energy balance in the transverse direction, and (2) an axial

slice of area Bdx, used to establish the streamwise energy balance along the refrigerant flow direction.

The derivation proceeds by first analyzing heat transfer in the transverse direction and subsequently coupling it with the longitudinal energy balance, leading to the development of a generalized expression for the LMTD in the cross-flow configuration.

Considering an energy balance over the differential control volume $dx \cdot dy$, the heat transfer from the refrigerant to the fluid stream in the y-direction is given by

$$U\left(T_r\left(x\right)-T_f\left(x,y\right)\right)dxdy = C_f \frac{dx}{L} dT_f \tag{25}$$

Canceling dx from both sides and rearranging (given that T_r is independent of y):

$$\frac{dT_f}{T_f - T_r\left(x\right)} = -\frac{UL}{C_f} dy \tag{26}$$

This first-order linear ordinary differential equation describes the fluid temperature variation in the transverse direction. Solving Eq.(26) with boundary conditions $T_f(x,0) = T_{f,in}$ yields

$$T_f\left(x,y\right) = T_r\left(x\right) - \left(T_r\left(x\right) - T_{f,in}\right)\exp\left(-\frac{UL}{C_f}\cdot y\right) \tag{27}$$

At the outlet of the fluid path ($y = B$), the local fluid exit temperature becomes

$$T_f\left(x,B\right) = T_r\left(x\right) - \left(T\left(x\right)_r - T_{f,in}\right)\exp\left(-\mathrm{NTU}\right) \tag{28}$$

where $\mathrm{NTU} = \dfrac{ULB}{C_f} = \dfrac{UA_{HX}}{C_f}$.

Next, we consider an energy balance over an infinitesimal streamwise element of area Bdx. The heat transferred to the fluid is expressed as

$$dQ = C_f \frac{dx}{L}\left(T_f\left(x,B\right) - T_{f,in}\right) \tag{29}$$

On the refrigerant side, when considering both the temperature glide characteristic of zeotropic mixtures and the pressure drop along the flow path, the heat gain can be evaluated by rearranging Eq. (13) as follows

$$dQ = -C_r \left(dT_r - \Delta T_{sat} \frac{dA}{A_{HX}} \right) \tag{30}$$

Equating Eqs. (29) and (30), and substituting Eq. (28), we obtain

$$\phi\left(\exp\left(-\mathrm{NTU}\right)-1\right)\left(T_r\left(x\right)-T_{f,in}\right)\frac{dx}{L}+\Delta T_{sat}\frac{dx}{L}-dT_r=0 \tag{31}$$

To simplify the governing equation, we define the following quantities

$$\xi = \frac{x}{L}, \theta\left(x\right) = T_r\left(x\right) - T_{f,in}, \psi = \phi\left(1-\exp\left(-\mathrm{NTU}\right)\right)$$

Substituting into Eq. (31) results in

$$\frac{d\theta}{d\xi}+\psi\theta-\Delta T_{sat}=0 \tag{32}$$

Solving Eq. (32) with the boundary condition $\theta\left(0\right) = T_{r,in} - T_{f,in}$, the solution becomes

$$\theta\left(\xi\right) = \left(\theta\left(0\right) - \frac{\Delta T_{sat}}{\psi} \right) \exp\left(-\psi\xi\right) + \frac{\Delta T_{sat}}{\psi} \tag{33}$$

Evaluating at $\xi = 1$, we can obtain

$$\ln \frac{T_{r,out} - T_{f,in} - \dfrac{\Delta T_{sat}}{\psi}}{T_{r,in} - T_{f,in} - \dfrac{\Delta T_{sat}}{\psi}} = -\psi \tag{34}$$

Recognizing $\mathrm{NTU} = \dfrac{UA_{HX}}{C_f} = \dfrac{T_{f,out} - T_{f,in}}{LMTD}$ and rearranging Eq. (34), we can express LMTD explicitly

$$LMTD^{\text{cross}}_{\Delta T_g \neq 0, \Delta p \neq 0} = \frac{-\left(T_{f,out} - T_{f,in}\right)}{\ln\left(1 + \frac{1}{\phi}\ln\left(1 - \frac{T_{r,in} - T_{r,out}}{T_{r,in} - T_{f,in} - \frac{\Delta T_{sat}}{\phi\left(1 - \exp\left(-\text{NTU}\right)\right)}}\right)\right)} \tag{35}$$

The general expression for LMTD derived in Eq. (35) can be further examined under limiting conditions to verify its consistency with classical results. The following cases demonstrate that, under appropriate assumptions, the expression reduces to the conventional LMTD formulation for crossflow heat exchangers involving two-phase flow.

1. Negligible Pressure Drop with Temperature Glide Present

   When the pressure drop is negligible but a temperature glide exists (i.e., $\Delta p \approx 0$ and $\phi \neq 0$), Eq. (35) remains valid and simplifies to

$$LMTD^{\text{cross}}_{\Delta T_g \neq 0, \Delta p = 0} = \frac{-\left(T_{f,out} - T_{f,in}\right)}{\ln\left(1 + \frac{1}{\phi}\ln\left(1 - \frac{T_{r,in} - T_{r,out}}{T_{r,in} - T_{f,in}}\right)\right)} \tag{36}$$

   This is consistent with the classical LMTD formulation for a cross-flow heat exchanger with one fluid mixed and the other unmixed, treating the two-phase refrigerant as a single-phase fluid with a capacitance rate of C_r.

2. Negligible Temperature Glide

   When temperature glide is negligible ($\Delta T_g \to 0$), the only variation in refrigerant temperature is due to pressure drop such that $T_{r,out} - T_{r,in} = \Delta T_{sat}$ In this limit, the LMTD expression simplifies considerably. As $\phi \to 0$, the argument of the inner logarithm in the denominator of Eq. (35) approaches unity. Applying the first-order approximation $\ln(1+X) \approx X$ for small X, the

inner logarithm reduces to $\dfrac{T_{r,out}-T_{r,in}}{T_{r,in}-T_{f,in}-\dfrac{T_{r,out}-T_{r,in}}{\phi\left(1-\exp\left(-\mathrm{NTU}\right)\right)}}$. Substituting this into Eq. (35), the entire expression inside the outer logarithm simplifies as

$$1+\frac{1}{\phi}\frac{T_{r,out}-T_{r,in}}{T_{r,in}-T_{f,in}-\dfrac{T_{r,out}-T_{r,in}}{\phi\left(1-\exp\left(-\mathrm{NTU}\right)\right)}}\sim\exp\left(-\mathrm{NTU}\right) \tag{37}$$

Therefore, the modified LMTD expression reduces to

$$\lim_{\phi\to 0} LMTD^{\mathrm{cross}}_{\Delta T_g\neq 0,\Delta p=0}=\frac{T_{f,out}-T_{f,in}}{\mathrm{NTU}} \tag{38}$$

This shows that, in the limiting case of negligible glide and dominant pressure-drop-induced temperature difference, the LMTD becomes linearly proportional to the fluid-side temperature change and inversely proportional to NTU.

We can further simplify this expression using the NTU definition from Eq. (28)

$$\mathrm{NTU}=-\ln\frac{T_r\left(x\right)-T_f\left(x,B\right)}{T_r\left(x\right)-T_{f,in}} \tag{39}$$

This relation holds at any axial location x. From Eq. (8), refrigerant temperature can be assumed to be linear when $\Delta T_{\mathrm{g}}\to 0$. We evaluate it at $x = L/2$, yielding

$$T_r\left(x=\frac{L}{2}\right)=\frac{T_{r,in}+T_{r,out}}{2} \tag{40}$$

At the same time, we can express the corresponding relationship as

$$T_f\left(x=\frac{L}{2},B\right)=T_{f,out} \tag{41}$$

based on the following

$$
\begin{aligned}
T_{f,out} &= \frac{1}{L}\int_0^L T_f\left(x,B\right)dx \\
&= \frac{T_{r,in}+T_{r,out}}{2} - \left(\frac{T_{r,in}+T_{r,out}}{2} - T_{f,in}\right)\exp\left(-\mathrm{NTU}\right) \\
&= T_f\left(x=\frac{L}{2},B\right)
\end{aligned}
\tag{42}
$$

Incorporating this midpoint evaluation into the NTU formulation, the expression becomes

$$
\mathrm{NTU} = -\ln\frac{\dfrac{T_{r,in}+T_{r,out}}{2} - T_{f,out}}{\dfrac{T_{r,in}+T_{r,out}}{2} - T_{f,in}} \tag{43}
$$

As a result, the LMTD can be expressed as

$$
LMTD^{\mathrm{cross}}_{\Delta T_g=0,\Delta p\neq 0} = \frac{-\left(T_{f,out}-T_{f,in}\right)}{\ln\left(\dfrac{\left(T_{r,in}+T_{r,out}\right)/2 - T_{f,out}}{\left(T_{r,in}+T_{r,out}\right)/2 - T_{f,in}}\right)} \tag{44}
$$

In particular, when there is negligible pressure drop, the refrigerant temperature remains constant across the heat exchanger, i.e., $T_r(x) = T_r$. In this case, the LMTD further simplifies to

$$
LMTD^{\mathrm{cross}}_{\Delta T_g=0,\Delta p=0} = \frac{-\left(T_{f,out}-T_{f,in}\right)}{\ln\left(\dfrac{T_r - T_{f,out}}{T_r - T_{f,in}}\right)} \tag{45}
$$

This expression corresponds to the classical LMTD formula for crossflow configurations in two-phase systems with constant refrigerant temperature.

3. Modified effectiveness-NTU method

While the LMTD method offers a direct approach for evaluating heat exchanger performance when inlet and outlet temperatures are known, it becomes less practical in scenarios involving phase change, strong temperature glide, or significant pressure drop—conditions under which outlet temperatures are not readily available. In such cases, the effectiveness–NTU method

provides a more versatile alternative. This method enables the prediction of thermal performance based on inlet conditions and heat exchanger geometry, making it especially useful for design and optimization studies. The following section extends the traditional NTU framework to accommodate two-phase systems with non-negligible temperature glide and pressure drop, providing a unified analytical expression for parallel-flow, counter-flow, and cross-flow configurations.

To proceed, we first revisit the basic definition of effectiveness as it forms the foundation of the NTU method. The effectiveness, ε, of a heat exchanger is defined as the ratio of the actual heat transfer rate to the maximum possible heat transfer rate. In the presence of phase change, the heat capacity rate of the two-phase fluid is typically much larger (or effectively infinite), so the capacitance of the single-phase stream governs the maximum possible heat transfer.

Accordingly, the effectiveness can be defined as

$$\varepsilon = \frac{T_{f,out} - T_{f,in}}{T_{r,in} - T_{f,in}} \tag{46}$$

3.1 Parallel-flow and counter-flow configurations

Consider a parallel-flow heat exchanger as illustrated in Fig. 2. Based on the temperature difference relations in Eq. (21), one can obtain

$$\frac{T_{r,out} - T_{f,out} + \beta/\alpha}{T_{r,in} - T_{f,in} + \beta/\alpha} = \exp\left(-\left(\phi + 1\right)\mathrm{NTU}\right) \tag{47}$$

Rewriting the left-hand side of Eq. (47) to isolate effectiveness, we obtain

$$\frac{T_{r,out} - T_{f,out} + \beta/\alpha}{T_{r,in} - T_{f,in} + \beta/\alpha} = \frac{\dfrac{T_{r,out} - T_{r,in}}{T_{r,in} - T_{f,in}} - \varepsilon}{1 + \dfrac{\beta}{\alpha}\dfrac{1}{T_{r,in} - T_{f,in}}} + 1 \tag{48}$$

Based on Eq. (11), refrigerant temperature change can be related to heat transfer and pressure drop. The refrigerant temperature difference can be written as

$$T_{r,out} - T_{r,in} = \Delta T_{sat} - \frac{1}{C_r} Q_{HX} \tag{49}$$

Applying an energy balance on the single-phase fluid side yields

$$Q_{HX} = C_f \left(T_{f,out} - T_{f,in} \right) \tag{50}$$

Substituting Eq. (50) into Eq. (49), the refrigerant-side temperature change becomes

$$T_{r,out} - T_{r,in} = \Delta T_{sat} - \phi \left(T_{f,out} - T_{f,in} \right) \tag{51}$$

Substituting Eq. (51), along with the definition of α and β, into Eq. (48) allows us to rewrite the left-hand side of Eq. (47) entirely in terms of known variables and ε, leading to

$$\frac{T_{r,out} - T_{f,out} + \beta/\alpha}{T_{r,in} - T_{f,in} + \beta/\alpha} = \frac{\gamma - (\phi+1)\varepsilon}{1 - \gamma/\left((\phi+1)\mathrm{NTU}\right)} + 1 \tag{52}$$

where a new dimensionless parameter is introduced as $\gamma = \Delta T_{sat}/(T_{r,in} - T_{f,in})$. This parameter γ quantifies the relative influence of refrigerant pressure drop. In general, ΔT_{sat} is negative due to the pressure drop along the refrigerant flow path, which causes a reduction in saturation temperature. For condensers, the temperature difference $T_{r,in} - T_{f,in}$ is typically positive, whereas for evaporators it is negative. Consequently, the dimensionless parameter γ assumes a negative value in condensation processes and a positive value in evaporation processes.

Equating Eq. (52) and Eq. (47) and solving for ε yields the expression for effectiveness in the parallel-flow configuration

$$\varepsilon^{\text{parallel}}_{\Delta T_g \neq 0, \Delta p \neq 0} = \frac{\gamma + \left(1 - \gamma/\left((\phi+1)\mathrm{NTU}\right)\right)\left(1 - \exp\left(-(\phi+1)\mathrm{NTU}\right)\right)}{\phi+1} \tag{53}$$

A similar procedure can be applied to the counter-flow configuration. Based on Eq. (21), the corresponding NTU-based expression is one can obtain

$$\frac{T_{r,out}-T_{f,in}+\beta/\alpha}{T_{r,in}-T_{f,out}+\beta/\alpha}=\exp\left(-\left(\phi-1\right)\mathrm{NTU}\right) \tag{54}$$

Rearranging the left-hand side of Eq. (54) and expressing all terms in terms of ε and γ, we obtain

$$\frac{T_{r,out}-T_{f,in}+\beta/\alpha}{T_{r,in}-T_{f,out}+\beta/\alpha}=\frac{\gamma-\phi\varepsilon+1+\gamma/\left(\alpha A\right)}{1-\varepsilon+\gamma/\left(\alpha A\right)} \tag{55}$$

Substituting Eq. (55) into Eq. (54) and solving for ε, the effectiveness expression for counter-flow becomes

$$\varepsilon^{\mathrm{counter}}_{\Delta T_g\neq 0,\Delta p\neq 0}=\frac{1+\gamma/\left(\left(1-\phi\right)\mathrm{NTU}\right)-\left(\gamma+\gamma/\left(\left(1-\phi\right)\mathrm{NTU}\right)+1\right)\exp\left(-\left(1-\phi\right)\mathrm{NTU}\right)}{1-\phi\exp\left(-\left(1-\phi\right)\mathrm{NTU}\right)} \tag{56}$$

In the limiting case where temperature glide is negligible ($C_\mathrm{r}\to\infty$, hence $\phi\to 0$), these expressions reduce to

$$\varepsilon^{\mathrm{parallel}}_{\Delta T_g=0,\Delta p\neq 0}=\left(1-\exp\left(-\mathrm{NTU}\right)\right)\left(1-\frac{\gamma}{\mathrm{NTU}}\right)+\gamma \tag{57}$$

$$\varepsilon^{\mathrm{counter}}_{\Delta T_g=0,\Delta p\neq 0}=\left(1-\exp\left(-\mathrm{NTU}\right)\right)\left(1+\frac{\gamma}{\mathrm{NTU}}\right)-\gamma\exp\left(-\mathrm{NTU}\right) \tag{58}$$

When refrigerant pressure drop is neglected ($\Delta T_\mathrm{sat}\to 0$, hence $\gamma\to 0$), Eqs. (53) and (56) reduce to the standard effectiveness expressions for parallel-flow and counter-flow configurations, respectively, as if the refrigerant behaves as a single-phase fluid with finite capacitance C_r. Furthermore, when both refrigerant pressure drop and temperature glide are negligible, the resulting expressions converge to the classical effectiveness–NTU relations with a constant two-phase temperature, irrespective of the heat exchanger configuration

$$\varepsilon_{\Delta T_g=0,\Delta p=0}=1-\exp\left(-\mathrm{NTU}\right) \tag{59}$$

When NTU → ∞, the effectiveness of the parallel-flow configuration asymptotically approaches

$$\lim_{\mathrm{NTU}\to\infty} \varepsilon^{\mathrm{parallel}}_{\Delta T_g \neq 0, \Delta p \neq 0} = \frac{1+\gamma}{1+\phi} \tag{60}$$

For condensation, where the pressure drop induces a decrease in saturation temperature, $\gamma < 0$, and the asymptotic effectiveness remains less than unity, as expected. For evaporation, $\gamma > 0$. In such cases, the effectiveness can exceed unity, indicating that the fluid outlet temperature may fall below the refrigerant inlet temperature. While this may seem non-physical under classical assumptions, it is consistent with the thermodynamic behavior of systems experiencing significant pressure drop.

For the counter-flow configuration, the effectiveness approaches unity as NTU increases, consistent with the classical behavior.

$$\lim_{\mathrm{NTU}\to\infty} \varepsilon^{\mathrm{counter}}_{\Delta T_g \neq 0, \Delta p \neq 0} = 1 \tag{61}$$

One might argue that the definition of effectiveness could be modified to constrain it to values below one. However, for the sake of consistency and direct comparison with the classical formulation, we retain the original definition of effectiveness throughout this study.

3.2 Crossflow configuration

Starting from the modified NTU relation for crossflow geometry, as given by Eq. (34), we obtain

$$\frac{T_{r,out} - T_{f,in} - \dfrac{\Delta T_{sat}}{\psi}}{T_{r,in} - T_{f,in} - \dfrac{\Delta T_{sat}}{\psi}} = \exp(-\psi) \tag{62}$$

Applying a series of substitutions and simplifications analogous to those used in the parallel-flow and counter-flow cases, the left-hand side of Eq. (62) can be reformulated as

$$\frac{T_{r,out}-T_{f,in}-\dfrac{\Delta T_{sat}}{\psi}}{T_{r,in}-T_{f,in}-\dfrac{\Delta T_{sat}}{\psi}}=\frac{T_{r,out}-T_{r,in}}{T_{r,in}-T_{f,in}-\dfrac{\Delta T_{sat}}{\psi}}+1 \tag{63}$$

Next, substituting Eq. (51) into Eq. (63) and isolating the effectiveness ε yields

$$\frac{T_{r,out}-T_{f,in}-\dfrac{\Delta T_{sat}}{\psi}}{T_{r,in}-T_{f,in}-\dfrac{\Delta T_{sat}}{\psi}}=\frac{\gamma-\phi\varepsilon}{1-\dfrac{\gamma}{\psi}}+1 \tag{64}$$

Finally, equating Eq. (64) with Eq. (62) and solving for ε results in the following expression for the effectiveness in the crossflow configuration with mixed refrigerant and unmixed secondary fluid

$$\varepsilon^{\text{cross}}_{\Delta T_g\neq 0,\Delta p\neq 0}=\frac{1}{\phi}\left(\gamma+\left(1-\frac{\gamma}{\phi\left(1-\exp\left(-\text{NTU}\right)\right)}\right)\left(1-\exp\left(-\phi\left(1-\exp\left(-\text{NTU}\right)\right)\right)\right)\right) \tag{65}$$

This formulation accounts for the combined effects of refrigerant pressure drop and temperature glide, providing a generalized NTU-based effectiveness relation applicable to two-phase crossflow systems.

Similarly, we can verify the consistency of the derived expression by examining several limiting cases. First, consider the case where refrigerant pressure drop is negligible, i.e., $\gamma\rightarrow 0$. In this limit, Eq. (65) simplifies directly to

$$\varepsilon^{\text{cross}}_{\Delta T_g\neq 0,\Delta p=0}=\frac{1}{\phi}\left(1-\exp\left(-\phi\left(1-\exp\left(-\text{NTU}\right)\right)\right)\right) \tag{66}$$

Next, in the absence of temperature glide ($\phi \rightarrow 0$), the limiting behavior must be approached more carefully. To facilitate this analysis, we define $\kappa=1-\exp\left(-\text{NTU}\right)$, and expand the exponential term $\exp(-\phi\kappa)$ using a second-order Taylor series,

$$\exp\left(-\phi\kappa\right)=1-\phi\kappa+\frac{\left(\phi\kappa\right)^2}{2}+\kappa^2 o\left(\phi^2\right) \tag{67}$$

Substituting this expansion into Eq. (65) allows it to be rewritten in the form

$$\begin{aligned}\varepsilon^{\text{cross}}_{\Delta T_g\neq 0,\Delta p\neq 0}&=\frac{1}{\phi}\left(\gamma+\left(1-\frac{\gamma}{\phi\kappa}\right)\left(\phi\kappa-\frac{\left(\phi\kappa\right)^2}{2}+\kappa^2 o\left(\phi^2\right)\right)\right)\\&\approx\frac{1}{\phi}\left(\phi\kappa\left(1+\frac{\gamma}{2}\right)-\frac{\left(\phi\kappa\right)^2}{2}+\kappa o\left(\phi\right)\right)\\&=\kappa\left(1+\frac{\gamma}{2}\right)-\frac{\kappa^2}{2}\phi+\kappa\frac{o\left(\phi\right)}{\phi}\end{aligned} \tag{68}$$

As $\phi\to 0$, the term $\dfrac{o\left(\phi\right)}{\phi}$ tends to zero, and the expression for effectiveness reduces to

$$\varepsilon^{\text{cross}}_{\Delta T_g=0,\Delta p\neq 0}=\left(1-\exp\left(-\text{NTU}\right)\right)\left(1+\frac{\gamma}{2}\right) \tag{69}$$

Finally, in the combined limit of negligible pressure drop and vanishing temperature glide, Eq. (69) further simplifies to

$$\varepsilon^{\text{cross}}_{\Delta T_g=0,\Delta p=0}=1-\exp\left(-\text{NTU}\right) \tag{70}$$

This final expression coincides with the classical NTU formulation for a heat exchanger with a constant two-phase temperature, thereby validating the consistency of the modified effectiveness relation under appropriate limiting conditions.

4. Results and discussion

4.1 Parallel-flow and counter-flow configurations

While previous studies have primarily focused on temperature gradients or overall effectiveness, the curvature of temperature profiles (whether they are convex or concave) has rarely been addressed, especially in the context of two-phase systems with temperature glide and pressure drop. However, analyzing curvature provides deeper physical insight into how these

effects shape the local thermal behavior along the heat exchanger. In particular, the curvature reveals important asymmetries between the refrigerant and fluid sides and offers a clear explanation for the performance deviations observed when pressure drop and glide are omitted from the analysis.

To explore these effects, we first examine the local temperature difference between the refrigerant and fluid under both the modified (i.e., corrected) and classical (i.e., uncorrected) formulations. When pressure drop and temperature glide are accounted for, the local temperature difference at an arbitrary location $A = A_x$ in a parallel-flow configuration is expressed using Eqs. (11) and (12) as

$$\Delta T_{x,\mathrm{mod}} = T_r - T_f = T_{r,in} - T_{f,in} + \frac{\Delta T_{sat}}{A_{HX}} A_x - \left(\frac{1}{C_r} + \frac{1}{C_f} \right) Q_x \tag{71}$$

where $Q_\mathrm{x} = C_\mathrm{f}(T_\mathrm{f,x} - T_\mathrm{f,in})$ represents the heat transferred from the inlet $A = 0$ to position $A = A_\mathrm{x}$. In contrast, when these effects are neglected, the standard LMTD method treats the two-phase refrigerant as an equivalent single-phase fluid, characterized by inlet and outlet temperatures with $T_\mathrm{r,in}$ and $T_\mathrm{r,out}$, respectively. The thermal capacitance of this simplified "single-phase" representation becomes

$$C_{r,SP} = \frac{C_f \left(T_{f,out} - T_{f,in} \right)}{\left(T_{r,in} - T_{r,out} \right)} \tag{72}$$

where the subscript "SP" indicates that the two-phase refrigerant is treated as a single-phase fluid. The local temperature difference predicted by the classical formulation is

$$\Delta T_{x,\mathrm{cl}} = T_{r,in} - T_{f,in} - \left(\frac{1}{C_{r,SP}} + \frac{1}{C_f} \right) Q_x \tag{73}$$

We define the local temperature difference error between the modified and classical formulations as

$$\Delta T_{x,dev} = \Delta T_{x,\mathrm{mod}} - \Delta T_{x,\mathrm{cl}} \tag{74}$$

Subtracting Eqs. (71) and (73), and using $Q_{\mathrm{x}} = C_{\mathrm{f}}(T_{\mathrm{f,x}} - T_{\mathrm{f,in}})$, we obtain

$$\Delta T_{x,dev} = \frac{\Delta T_{sat}}{A_{HX}} A_x + \left(\frac{1}{C_{r,SP}} - \frac{1}{C_r} \right) C_f \left(T_{f,x} - T_{f,in} \right) \tag{75}$$

Substituting the expression for $C_{\mathrm{r,SP}}$ from Eq. (72) into Eq. (75) and rearranging terms gives

$$\Delta T_{x,dev} = \frac{\Delta T_{sat}}{A_{HX}} A_x + \left(\frac{T_{r,in} - T_{r,out}}{T_{f,out} - T_{f,in}} - \phi \right) \left(T_{f,x} - T_{f,in} \right) \tag{76}$$

Recalling Eq. (51), which relates the refrigerant temperature change to the total saturation temperature shift and the fluid-side temperature rise scaled by the capacitance ratio ϕ, and substituting it into Eq. (76), we arrive at the following compact form

$$\Delta T_{x,dev} = \left(\frac{A_x}{A_{HX}} - \frac{T_{f,x} - T_{f,in}}{T_{f,out} - T_{f,in}} \right) \Delta T_{sat} \tag{77}$$

A similar derivation for the counter-flow configuration gives

$$\Delta T_{x,dev} = \left(\frac{A_x}{A_{HX}} - \frac{T_{f,out} - T_{f,x}}{T_{f,out} - T_{f,in}} \right) \Delta T_{sat} \tag{78}$$

Before evaluating the error introduced by these simplifications, we examine the curvature of the temperature profiles of both refrigerant and fluid. To do so, we obtain the second derivatives of their temperatures with respect to heat exchanger area by differentiating Eqs. (11) and (12) twice

$$\frac{d^2 T_r}{dA^2} = -\frac{1}{C_r} \frac{d^2 Q}{dA^2} \tag{79}$$

$$\frac{d^2 T_f}{dA^2} = \pm \frac{1}{C_f} \frac{d^2 Q}{dA^2} \tag{80}$$

where the upper and lower signs correspond to the parallel-flow and counter-flow configurations, respectively. Recalling that $\frac{dQ}{dA} = U\Delta T$ and ΔT represents the local temperature difference between the refrigerant and the fluid, the second derivatives of the fluid and refrigerant temperatures with respect to heat exchanger area are given by

$$\frac{d^2T_r}{dA^2} = -\frac{U}{C_r}\frac{d\Delta T}{dA} \tag{81}$$

$$\frac{d^2T_f}{dA^2} = \pm\frac{U}{C_f}\frac{d\Delta T}{dA} \tag{82}$$

From Eq. (17), the first derivative of the local temperature difference with respect to heat exchanger area can be readily obtained as:

$$\frac{d\Delta T}{dA} = \alpha\Delta T + \frac{\Delta T_{sat}}{A_{HX}} \tag{83}$$

Substituting Eq. (83) into Eqs. (81) and (82) yields

$$\frac{d^2T_r}{dA^2} = \begin{cases} \dfrac{U^2}{C_rC_f}\left(\left(\phi+1\right)\Delta T - \dfrac{\Delta T_{sat}}{\mathrm{NTU}}\right), \text{ for parallel flow} \\ \dfrac{U^2}{C_rC_f}\left(\left(\phi-1\right)\Delta T - \dfrac{\Delta T_{sat}}{\mathrm{NTU}}\right), \text{ for counter flow} \end{cases} \tag{84}$$

$$\frac{d^2T_f}{dA^2} = \begin{cases} -\left(\dfrac{U}{C_f}\right)^2\left(\left(\phi+1\right)\Delta T - \dfrac{\Delta T_{sat}}{\mathrm{NTU}}\right), \text{ for parallel flow} \\ \left(\dfrac{U}{C_f}\right)^2\left(\left(\phi-1\right)\Delta T - \dfrac{\Delta T_{sat}}{\mathrm{NTU}}\right), \text{ for counter flow} \end{cases} \tag{85}$$

By examining Eqs. (84) and (85), the curvature characteristics of refrigerant (T_r) and fluid (T_f) temperature profiles can be determined for both parallel-flow and counter-flow configurations during condensation and evaporation. These results are summarized in Table 1. For parallel flow,

the fluid temperature profile always exhibits curvature opposite to that of the refrigerant. In contrast, for counter-flow, the fluid and refrigerant temperature profiles exhibit the same curvature. The curvature depends on the capacitance ratio ϕ and saturation temperature change ΔT_{sat}, and has important implications for local heat transfer behavior and the accuracy of simplified thermal models.

In most practical cases involving two-phase refrigerant flow, the capacitance ratio is very small, i.e., $\phi << 1$. Under these conditions, for the counter-flow configuration, the temperature profiles of both the refrigerant and the secondary fluid exhibit characteristic curvatures that persist even when pressure drop is taken into account. Specifically, during condensation, the refrigerant temperature profile is typically concave, while it becomes convex during evaporation.

Furthermore, the temperature profile of the secondary fluid is generally concave during condensation and convex during evaporation, regardless of the flow arrangement. These curvature characteristics are primarily driven by the nonlinear enthalpy–temperature relationship of zeotropic mixtures and the evolving temperature difference along the heat exchanger surface.

With the help of the curvature of the temperature profiles shown in Fig. 5 through Fig. 8, we can assess the deviation introduced by classical LMTD assumptions when applied to zeotropic refrigerants during condensation. For the parallel-flow case (Fig. 5 and Fig. 6), a geometric inspection of the temperature profiles reveals

$$\frac{T_{f,x} - T_{f,in}}{T_{f,out} - T_{f,in}} = \frac{A^*}{A_{HX}} > \frac{A_x}{A_{HX}} \tag{86}$$

For the counter-flow configuration (Fig. 7 and Fig. 8), a similar inspection reveals

$$\frac{T_{f,out} - T_{f,x}}{T_{f,out} - T_{f,in}} = \frac{A^*}{A_{HX}} < \frac{A_x}{A_{HX}} \tag{87}$$

Therefore, by combining Eqs, (76) and (78), we obtain

$$\Delta T_{x,\mathrm{mod}} \geq \Delta T_{x,\mathrm{cl}} \text{ for parallel-flow, } \Delta T_{x,\mathrm{mod}} \leq \Delta T_{x,\mathrm{cl}} \text{ for counter-flow} \tag{88}$$

These inequalities reveal a fundamental asymmetry: when pressure drop is present, the classical LMTD method underestimates the local temperature difference in the parallel-flow configuration and overestimates it in the counter-flow configuration. The equalities hold only when pressure drop is negligible, further confirming the consistency of the modified formulation with the classical model under limiting conditions, and reinforcing the observations made in earlier discussions. As a result, the classical LMTD method tends to underpredict the thermal performance of parallel-flow heat exchangers and overpredict that of counter-flow heat exchangers.

To quantify the errors introduced by neglecting pressure drop and temperature glide in the LMTD calculation, Eq. (24) is approximated using a second-order Taylor expansion. Let *f* denote the classical LMTD

$$f\left(\Delta T_1, \Delta T_2\right) = \frac{\Delta T_1 - \Delta T_2}{\ln \dfrac{\Delta T_1}{\Delta T_2}} \tag{89}$$

The error between the modified and classical LMTD, denoted as δ_{LMTD}, can be approximated as

$$\begin{aligned} \delta_{LMTD} &= LMTD_{\mathrm{mod}} - LMTD_{\mathrm{cl}} \\ &= f\left(\Delta T_1 + \frac{\beta}{\alpha}, \Delta T_2 + \frac{\beta}{\alpha}\right) - \frac{\beta}{\alpha} - f\left(\Delta T_1, \Delta T_2\right) \\ &\approx \frac{\beta}{\alpha}\left(\frac{f^2}{\Delta T_1 \Delta T_2} - 1\right) + \left(\frac{\beta}{\alpha}\right)^2 \frac{1}{\Delta T_2}\left(\frac{f}{\Delta T_1} - \frac{1}{2} - \frac{1}{2}\frac{\Delta T_2}{\Delta T_1}\right)\frac{f^2}{\Delta T_1 \Delta T_2} \end{aligned} \tag{90}$$

It can be observed that the LMTD error is primarily governed by the ratio $\Delta T_1/\Delta T_2$, as both $\dfrac{f^2}{\Delta T_1 \Delta T_2}$ and $\dfrac{f}{\Delta T_1}$ depend only on this ratio. Fig. 9 illustrates the relative errors between the corrected and uncorrected LMTD values, with ΔT_2 fixed at 1 K. In the figure, solid and dashed lines represent the parallel-flow and counter-flow configurations, respectively.

Without accounting for pressure drop and temperature glide, the classical (uncorrected) LMTD method underpredicts the performance of parallel-flow heat exchangers and overpredicts that of counter-flow heat exchangers. The relative error increases significantly with increasing $\Delta T_1/\Delta T_2$, and the counter-flow configuration appears more sensitive to this variation. For instance, when $\Delta T_1/\Delta T_2 = 10$, the relative error surpasses 15% in the counter-flow configuration and 7% in the parallel-flow case, underscoring the limitations of the classical formulation under non-ideal conditions. This also indicates that the counter-flow configuration is more sensitive to thermal asymmetries introduced by pressure drop and temperature glide.

According to Eq. (24), an increase in pressure drop increases β, while an increase in temperature glide decreases α. Since the error depends on the ratio β/α, increases in either effect—or both—amplify the deviation between the corrected and classical LMTD, confirming that the traditional LMTD method can lead to substantial inaccuracies in systems with significant pressure drop and temperature glide.

Figs. 10 and 11 show the effectiveness ε of parallel-flow and counter-flow condensers, respectively, at a low capacitance ratio $\phi = 0.02$. When pressure drop and temperature glide are neglected, the refrigerant is treated as having a constant saturation temperature throughout the heat exchanger. This simplification leads to an artificially elevated mean temperature difference between the refrigerant and the fluid, resulting in an overestimation of heat transfer. In reality, both pressure drop and temperature glide cause the refrigerant temperature to decrease along the flow path during condensation. This gradual cooling lowers the actual thermal driving force, thereby reducing the true heat transfer rate. As shown in the figures, increasing pressure drop results in a noticeable reduction in effectiveness, owing to the diminished temperature difference between the two streams. As a result, the classical LMTD method overpredicts effectiveness,

particularly at large NTU values. The counter-flow configuration exhibits smaller errors because the temperature difference between the two streams is more uniformly distributed along the exchanger length. Even when pressure drop and glide are neglected, the error in the effective mean temperature difference is partially compensated by the counter-flow arrangement itself. This thermal symmetry makes the counter-flow geometry more robust to such simplifications, resulting in smaller discrepancies between the corrected and classical predictions.

Figs. 12 and 13 extend this analysis to a higher capacitance ratio of $\phi = 0.5$, where the effect of temperature glide becomes more pronounced. Compared to the $\phi = 0.02$ cases, both parallel- and counter-flow configurations exhibit reduced effectiveness across all NTU values. An increase in temperature glide diminishes the temperature difference between the refrigerant and the fluid, thereby reducing the overall heat transfer potential. This reduction in thermal driving force is especially pronounced in the parallel-flow case (Fig. 12), where the co-directional flow offers limited capacity to offset asymmetries. In contrast, the counter-flow configuration (Fig. 13) experiences a smaller drop in effectiveness due to its ability to better accommodate non-uniform temperature profiles along the flow path.

A more nuanced interplay arises during evaporation, as illustrated in Figs. 14–17. In this regime, pressure drop and temperature glide influence the refrigerant temperature in opposite directions. Pressure drop leads to a decrease in saturation temperature along the refrigerant flow path, which increases the local temperature difference between the refrigerant and the fluid. This enhanced thermal gradient improves the overall heat transfer rate. As shown in the figures, increasing the pressure drop leads to a corresponding increase in effectiveness.

In contrast, temperature glide causes the refrigerant temperature to increase along the evaporating process at constant pressure, thereby reducing the temperature difference between the

refrigerant and the fluid. This diminished thermal driving force leads to lower heat transfer rates and a reduction in effectiveness. The net impact on performance depends on the relative magnitudes of pressure drop and glide, which in turn are governed by the system's thermal and hydraulic characteristics.

When the capacitance ratio ϕ is small (as in Figs. 14 and 15), this corresponds to a large refrigerant-side capacitance C_r, which implies that the temperature glide is relatively small. In this case, the effect of pressure drop dominates. The net result is that the corrected model predicts a higher effectiveness than the classical model. The refrigerant temperature profile under these conditions resembles that shown in Fig. 18, where a steep pressure drop and low ϕ cause a significant temperature decline along the refrigerant path.

This effect can be sufficiently strong that the effectiveness might exceed unity, particularly in parallel-flow evaporators. Physically, this occurs when the fluid outlet temperature falls below the refrigerant inlet temperature, a situation made possible by the significant refrigerant-side pressure drop. Although such a result would be impossible under constant refrigerant temperature assumptions, it is entirely plausible when pressure drop is properly accounted for, as it causes a downward shift in refrigerant temperature throughout the exchanger. This observation highlights the importance of accurately modeling pressure-dependent temperature changes in systems using zeotropic mixtures or undergoing significant evaporative pressure loss.

For larger capacitance ratios (ϕ = 0.5), as shown in Figs. 16 and 17, the refrigerant-side capacitance C_r is smaller, indicating that temperature glide becomes more pronounced. In this regime, the influence of temperature glide increasingly dominates over pressure drop.

Comparing Fig. 14 (ϕ = 0.02) and Fig. 16 (ϕ = 0.5) reveals that a larger temperature glide can significantly suppress the effectiveness in parallel-flow evaporators, particularly when the

refrigerant-side capacitance is no longer dominant. A similar trend is observed when comparing Figs. 15 and 17 for the counter-flow configuration: the effectiveness also decreases as the capacitance ratio increases. However, in the counter-flow case, the deviations between the corrected and classical predictions are generally less pronounced.

This is because in counter-flow heat exchangers, the fluid outlet temperature is thermodynamically bounded by the refrigerant inlet temperature, which remains fixed regardless of pressure drop or glide. This constraint inherently limits the maximum possible effectiveness and suppresses extreme deviations, even when pressure drop and temperature glide are considered. As a result, while increasing ϕ still reduces effectiveness, the impact of neglecting pressure drop and glide is partially mitigated by the asymptotic behavior of the outlet temperature, making the counter-flow configuration more resistant to modeling inaccuracies.

In extreme cases, the increase in refrigerant temperature along the flow path due to glide can no longer be fully offset by the cooling effect of pressure drop. As a result, the refrigerant temperature may exhibit a net increasing trend, reducing the local temperature difference between the two fluids. This behavior is qualitatively consistent with the scenario shown in Fig. 19 under conditions of large ϕ and small pressure drop, where thermal asymmetry leads to diminished driving temperature differences along the heat exchanger.

This comparison emphasizes the strong sensitivity of effectiveness to the capacitance ratio ϕ. As ϕ increases, the balancing effect of pressure drop becomes less effective in mitigating the glide-induced temperature rise. Therefore, accurately modeling both pressure drop and temperature glide is essential for predicting evaporator performance, especially in systems operating under high-glide refrigerants and moderate-to-high capacitance ratios.

Fig. 20 illustrates a possible scenario of temperature crossing in a counter-flow evaporator. In this case, the refrigerant initially has a higher temperature than the fluid and releases heat near the evaporator inlet. However, due to significant pressure drop, the refrigerant temperature decreases below that of the fluid further downstream, leading it to absorb heat in the latter portion of the exchanger. This reversal in heat transfer direction does not violate the second law of thermodynamics, as the refrigerant temperature change is driven predominantly by pressure effects, not by local energy exchange alone.

Under such conditions, it is possible for the fluid outlet temperature to fall below the refrigerant inlet temperature, a result that would be deemed unphysical under classical assumptions but is entirely plausible when pressure-induced temperature variation is considered. Naturally, as the evaporator size increases, the fluid outlet temperature will asymptotically approach the refrigerant inlet temperature, and the effectiveness will decrease toward unity, consistent with the behavior predicted by Eq. (61).

It is important to emphasize that both the standard LMTD method and the modified version proposed here become invalid when temperature crossing occurs, as they rely on the assumption of a monotonic and unidirectional temperature difference between the two fluid streams. To address this limitation, Qiao [20] developed an approach specifically designed to handle temperature crossing scenarios by introducing a smooth and differentiable extrapolation scheme. This approach classifies temperature profiles into seven representative cases and adjusts the LMTD calculation accordingly through interpolation, extrapolation, or a weighted combination of partial LMTDs, to enable robust and continuous heat transfer calculations even under transient conditions where temperature crossing is common. It is important to note that this framework does not impose limitations on the choice of LMTD formulation. Therefore, the modified LMTD

method proposed in this work remains fully applicable within this context and can reliably capture heat transfer performance in the presence of temperature crossing.

4.2 Cross-flow configuration

Following the analysis of parallel- and counter-flow configurations, we now shift focus to the cross-flow arrangement, where the refrigerant and fluid streams interact perpendicularly. The corrected LMTD formulation for cross-flow continues to incorporate the effects of temperature glide and pressure drop through the parameters ϕ and ΔT_{sat}, respectively. While these influences were previously characterized, their combined impact in cross-flow geometry introduces additional nonlinearities and requires separate examination due to the distinct flow structure.

In particular, the corrected cross-flow LMTD expression contains a glide-pressure correction term $\frac{\Delta T_{sat}}{\phi\left(1-\exp\left(-\mathrm{NTU}\right)\right)}$. This term is sensitive to both ϕ and NTU and becomes significantly amplified under the following conditions:

- When $\phi \ll 1$, corresponding to a large refrigerant-side thermal capacitance (as in two-phase conditions where $C_{\mathrm{r}} \to \infty$, the glide effect becomes dominant.
- When NTU is large, the exponential term vanishes, i.e., $1 - \exp(\text{-NTU}) \to 1$, and the correction reduces to $\Delta T_{\mathrm{sat}}/\phi$, reaching its maximum value.
- When NTU is small, $1 - \exp(\text{-NTU}) \ll 1$, and the denominator becomes very small, causing the correction term to grow rapidly and potentially dominate the LMTD expression.

Unlike the parallel-flow and counter-flow configurations, where the mathematical structure of the modified LMTD allows for closed-form error expressions, the cross-flow case is more analytically intractable. The corrected formulation involves a nested logarithmic structure in which the pressure-glide correction appears inside a product of logarithmic terms. This nonlinear coupling makes it difficult to isolate a simple symbolic expression for the error in terms of ϕ, NTU,

and ΔT_{sat}. Furthermore, the combined influence of these parameters can lead to multiple, non-monotonic behaviors depending on the specific operating conditions. For example, the error may be large for small ϕ and either low or high NTU, but the exact magnitude and direction of deviation vary case by case.

Given this complexity, we do not pursue a generalized analytical error expression for cross-flow. Instead, the error behavior is summarized qualitatively in Table 2, which outlines the dominant trends and sensitivities associated with key parameter regimes. This approach provides a practical framework for interpreting deviations from the standard LMTD and highlights conditions under which the corrected formulation becomes essential for accurate heat exchanger modeling.

Figs. 21–24 present the effectiveness of cross-flow heat exchangers under varying degrees of refrigerant pressure drop, represented by the parameter γ, for both condenser and evaporator configurations at two different capacitance ratios, $\phi = 0.02$ and $\phi = 0.5$. In each case, effectiveness is plotted as a function of NTU, with the baseline case (no pressure drop or temperature glide) included for reference. As in previous sections, pressure drop is incorporated through the dimensionless parameter $\gamma = \Delta T_{sat}/(T_{f,in}-T_{r,in})$, where $\gamma < 0$ for condensation and $\gamma > 0$ for evaporation.

Fig. 21 illustrates the effectiveness of a cross-flow condenser at a small capacitance ratio $\phi = 0.02$. As the magnitude of pressure drop increases (i.e., more negative γ), the effectiveness decreases across all NTU values. This trend is expected, as the pressure drop reduces the refrigerant saturation temperature along the flow path, lowering the driving temperature difference and diminishing heat transfer. The discrepancy grows with increasing NTU, where the classical method more significantly overpredicts performance. The results highlight the necessity of

incorporating pressure drop effects in systems where the two-phase refrigerant dominates the thermal capacity.

Fig. 22 presents the corresponding case for a cross-flow evaporator with the same low capacitance ratio. Here, pressure drop lowers the refrigerant temperature, thereby enhancing the local temperature difference and increasing the heat transfer rate. Consequently, the effectiveness improves with increasing γ, and the corrected prediction exceeds the classical formulation. This effect is most pronounced at high NTU, where the assumption of constant refrigerant temperature in the classical model leads to an underestimation of performance.

In Fig. 23, the performance of a condenser with a moderate capacitance ratio $\phi = 0.5$ is shown. A larger ϕ corresponds to a stronger influence of temperature glide, which raises the refrigerant temperature along the flow direction and reduces the effective temperature difference. As a result, effectiveness is lower compared to the $\phi = 0.02$ case. Comparing Figs. 21 and 23 clearly illustrates how an increase in ϕ—and thus stronger glide—diminishes the overall heat transfer effectiveness, even under the same pressure drop conditions.

Finally, Fig. 24 shows the effectiveness of a cross-flow evaporator at $\phi = 0.5$. In this case, the competing effects of pressure drop and temperature glide become more balanced. While pressure drop still enhances heat transfer by lowering the refrigerant saturation temperature, the elevated glide associated with higher ϕ offsets this benefit by increasing the refrigerant temperature during evaporation. As a result, the effectiveness gain due to pressure drop is reduced relative to the $\phi = 0.02$ case. These findings underscore that, in systems with significant temperature glide, both pressure drop and glide must be accurately accounted for to avoid substantial errors in effectiveness prediction.

4.3 Key Modeling Assumptions

In deriving the modified LMTD formulation, a linear variation of temperature glide within the two-phase region is assumed. This simplification enables analytical tractability and facilitates closed-form expressions in the reformulated LMTD and ε–NTU methods, while still capturing the dominant effects of glide on heat exchanger performance.

To evaluate the validity of this assumption, we examined two zeotropic refrigerant mixtures with large temperature glides, R-407C and R-454C, and analyzed their saturation temperature profiles over the two-phase region at representative operating pressures. As illustrated in Fig. 25 and Fig. 26, the saturation temperature curves, generated using the high-accuracy thermophysical property database REFPROP 10.0 [21], for both mixtures are generally smooth and exhibit nearly linear behavior with respect to vapor quality. While minor nonlinearity is present near the bubble and dew points, the deviation from linearity is typically small for most practical glide magnitudes. For example, R-407C and R-454C exhibit total temperature glides of approximately 6.2 K and 7.8 K, respectively, at 0.5 MPa. When comparing the actual saturation temperature curves to their linear approximations, the maximum deviations are approximately 0.07 K for R-407C and 0.24 K for R-454C, corresponding to relative errors of 1.1% and 3.1%, respectively.

Moreover, in practical systems, these local approximation errors are further mitigated over the entire flow path due to the averaging effects along the heat exchanger length—especially in long channels. These deviations translate into minimal errors in the local temperature difference that drives heat transfer, and therefore have negligible impact on the predicted heat transfer rate or exchanger effectiveness.

Based on this analysis, we conclude that the linear glide assumption is reasonable and introduces only minor errors, even for refrigerants with relatively large glides. In cases where the saturation temperature profile across the two-phase region is highly nonlinear, the proposed

method remains applicable through segmentation: the heat exchanger can be divided into small control volumes where glide is locally linear. The total heat transfer is then computed by summing contributions from all segments, preserving accuracy while retaining analytical simplicity.

A similar approach applies to the treatment of two-phase pressure drop. It is well understood that in general two-phase pressure drop is nonlinear due to evolving flow regimes, changing vapor quality, and variations in local thermophysical properties. This complexity often leads to the perception that two-phase pressure drop is inherently highly nonlinear. However, this nonlinearity is primarily pronounced when heat transfer is significant, i.e., during evaporation or condensation, since heat transfer alters the vapor quality, which in turn affects the pressure gradient along the flow path. In contrast, for adiabatic two-phase flows or in cases with modest heat transfer and moderate pressure drops, the pressure drop can exhibit approximately linear behavior along the length.

In this work, the total temperature variation of the refrigerant in the two-phase region is conceptually divided into two distinct contributions (as expressed in Eq. (7)): (1) the temperature change purely due to pressure drop (with no heat transfer), and (2) the temperature glide associated with heat transfer, which alters the vapor quality. These two components are decoupled in our formulation for analytical tractability. The assumption of linear pressure drop along the flow path in Eq. (9) serves as a first-order approximation to capture the dominant pressure trend while enabling closed-form integration in the modified LMTD and ε–NTU formulations. This simplification is consistent with system-level modeling practices, where detailed local flow structures are often unknown.

The potential error introduced by this assumption primarily affects the portion of the temperature profile induced by pressure drop alone. Since the majority of temperature variation

arises from the glide component due to heat transfer, which is already accounted for separately, this residual effect is expected to be small. To conservatively capture the pressure-induced temperature change, we bound this effect by using the average slopes of the dew and bubble point curves. This approach is generic and robust, especially when the inlet vapor quality is case-dependent and not known a priori.

To assess the impact of the linear pressure drop approximation, we conducted a comparative analysis using a nonlinear pressure drop profile calculated from empirical correlations such as the Friedel models. For a representative case involving R454C evaporating at 7 °C with a moderate pressure drop of ~50 kPa over a two-phase flow length of approximately 20 m, the total temperature change induced solely by pressure drop was around 1.7 K. This corresponds to a local temperature change of less than 0.1 K per meter, indicating that the linear approximation introduces minimal error over a long tube. Given such small gradients, assuming a linearly varying temperature due to pressure drop is justified and does not significantly distort the overall temperature profile. When pressure variation is strong or nonlinearities are expected, segmenting the heat exchanger into shorter zones ensures that the linear approximation remains valid locally, while still enabling the analytical framework to be used effectively.

In this study, we also assume a uniform overall heat transfer coefficient U along the entire heat exchanger for analytical tractability. However, the structure of the proposed formulation naturally lends itself to further refinement. It is important to note that this is not an additional assumption introduced by the modified formulations, instead it is inherited from the standard LMTD and ε–NTU approaches. In practice, real-world heat exchangers often exhibit significant spatial variation in local heat transfer coefficients and corresponding NTU values due to evolving boundary conditions, particularly near the inlet and outlet regions. Such variations are especially pronounced

in systems where heat and mass transfer are strongly coupled, e.g., in indirect evaporative cooling, membrane-based exchangers, or units handling zeotropic mixtures and refrigerant–oil blends. In these applications, the phase change behavior, fluid properties, and flow regimes can vary substantially along the length of the exchanger, leading to spatially non-uniform effectiveness. To account for such variations, again the segmental modeling approach can be applied, assigning local NTU, γ and glide values to each segment. This enhances model fidelity while leveraging the same analytical structure.

Although the formulations developed in this work are derived in the context of two-phase flow, we would like to clarify that the generalized analytical expressions, both the modified LMTD and ε–NTU methods, remain valid in single-phase regimes as well. In particular, single-phase flow can be treated as a special case of the proposed framework, characterized by zero temperature glide (due to the absence of phase change) and a well-defined thermal capacitance based on the specific heat of the single-phase fluid.

As shown earlier, the proposed equations reduce to the corresponding LMTD and ε–NTU formulations in the limit of zero temperature glide, confirming the generality and consistency of the approach across different flow regimes. This versatility supports a zonal modeling strategy, in which the heat exchanger is divided into three regions: single-phase liquid, two-phase, and single-phase vapor. The two-phase section employs the full modified formulation to account for temperature glide and pressure effects, while the single-phase regions use the same analytical structure with standard definitions of specific heat and temperature difference.

However, it is important to emphasize that applying either the standard or modified LMTD or ε–NTU method over the entire exchanger, when both single-phase and two-phase regions are present, may lead to inaccuracies. This is because such an approach assumes a uniform overall

heat transfer coefficient U, which may not hold across regions with significantly different flow regimes and thermal properties. Therefore, to maintain accuracy, each region should be analyzed separately, with appropriate local definitions of U, NTU, and fluid properties.

5. Conclusion

This study introduces a novel analytical reformulation of the classical Log Mean Temperature Difference (LMTD) and effectiveness–NTU methods to account for pressure drop and temperature glide in two-phase heat exchangers using zeotropic refrigerants. While conventional approaches assume idealized conditions, this work fills a critical research gap by systematically integrating two dominant non-ideal effects, i.e., pressure-induced saturation shifts and temperature glide, into closed-form performance models for parallel-flow, counter-flow, and cross-flow configurations.

Two dimensionless parameters are introduced: the glide strength parameter ϕ and the normalized saturation shift γ. These compactly capture the thermodynamic asymmetries that arise from zeotropic behavior and pressure losses. The modified models retain analytical tractability, reduce to classical solutions in limiting cases, and offer improved predictive accuracy across a broad range of operating conditions.

Results reveal that classical LMTD and ε–NTU methods can incur heat transfer prediction errors exceeding ±10% in parallel and counter flow, and up to 30% in cross-flow arrangements, especially under strong glide and pressure drop conditions. A curvature-based analysis of temperature profiles further explains the origins of these deviations and provides physical insight into how classical assumptions break down.

In contrast to prior studies that either neglect these effects or rely on numerical simulations, the present work offers a unified, fully analytical, and broadly applicable framework that bridges classical theory with real-world behavior in two-phase heat exchangers using zeotropic mixtures.

These findings provide a practical and theoretically rigorous foundation for accurate performance evaluation and design optimization under realistic operating conditions.

REFERENCES

[1] F.P. Incropera, D.P. Dewitt, T.L. Bergman, A.S. Lavin. Fundamentals of heat and mass transfer (6^{th} ed). John Wiley & Sons Inc., New Jersey, USA, 2007.

[2] L.C.M. Itard, C.H.M. Machielsen. Considerations when modelling compression/resorption heat pumps. Int. J. Refrig. 17 (1994) 453-460.

[3] P.G. Lundqvist. Analysis of plate type heat exchangers with zeotropic refrigerant blends. Heat Pump and Refrigeration System: Design, Analysis and Applications 34 (1995) 37-45.

[4] L.A. Schaefer, S.V. Shelton. Heat exchanger mean temperature differences for refrigerant mixtures. ASME International Mechanical Engineering Congress and Exposition, Anaheim, CA, USA, November 15–20, 1998, pp. 383–389.

[5] L. Rajapaksha. Influence of special attributes of zeotropic refrigerant mixtures on design and operation of vapour compression refrigeration and heat pump systems. Energy Convers. Manage. 48 (2007) 539-545.

[6] K.L. Wong, M.T. Ke, S.S. Ku. The log mean heat transfer rate metod for heat exchanger considering the influence of heat radiation. Energy Convers. Manage. 50 (2009) 2693-2698.

[7] X. Cui, K.J. Chua, M.R. Islam, W.M. Yang. Fundamental formulation of a modified LMTD method to study indirect evaporative heat exchangers. Energy Convers. Manage. 88 (2014) 372-381.

[8] J. Claesson. Correction of logarithmic mean temperature difference in a compact brazed plate evaporator assuming heat flux governed flow boiling heat transfer coefficient. Int. J. Refrig. 28 (2005) 573–578.

[9] M. Utamura, K. Nikitin, Y. Kato. Generalization of logarithmic mean temperature difference method for heat exchanger performance analysis. Therm. Sci. Eng. 15 (2007) 163–173.

[10] M. Mistry, R. Misener. Optimising heat exchanger network synthesis using convexity properties of the logarithmic mean temperature difference. Comput. Chem. Eng. 94 (2016) 1-17.

[11] G.F. Nellis, J.M. Pfotenhauer. Effectiveness-NTU relationship for a counterflow heat exchanger subjected to an external heat transfer. J. Heat Transf. 127 (2005) 1071-1073.

[12] A.B.S. Alquaity, S.A. Al-Dini, S.M. Zubair. Effectiveness-NTU relations for parallel flow heat exchangers: The effect of kinetic energy variation and heat leak from outside. Int. J. Refrig. 36 (2013) 1557-1569.

[13] C.Q. Ren. Corrections to the simple effectiveness-NTU method for counterflow cooling towers and packed bed liquid desiccant–air contact systems. Int. J. Heat Mass Transf. 51 (2008) 237-245.

[14] C.Q. Ren. Effectiveness–NTU relation for packed bed liquid desiccant–air contact systems with a double film model for heat and mass transfer. Int. J. Heat Mass Transf. 51 (2008) 1793-1803.

[15] A.J. Fix, J.E. Braun, D.M. Warsinger. A general effectiveness-NTU modeling framework for membrane dehumidification systems. Appl. Therm. Eng. 236 (2024) 121514.

[16] Y. Tang, Z. Wang, W. Lyu. An improved effectiveness-NTU method for streamlining the design and optimization of packed bed latent thermal energy storage. Sustain. Cities Soc. 100 (2024) 105034.

[17] M.K. Mansour. Practical effectiveness-NTU model for cooling and dehumidifying coil with non-unit Lewis Factor. Appl. Therm. Eng. 100 (2016) 1111-1118.

[18] Y. Xie, Z. Xu, N. Mei. Evaluation of the effectiveness-NTU method for countercurrent humidifier. Appl. Therm. Eng. 99 (2016) 1270-1276.

[19] W. Asvapoositkul, M. Kuansathan. The effectiveness-NTU approach for evaluation of an air-cooled heat exchanger. Heat Transf. Eng. 37 (2016) 140-149.

[20] H. Qiao. Transient modeling of two-stage and variable refrigerant flow vapor compression systems with frosting and defrosting. PhD Dissertation, University of Maryland, College Park, 2014.

[21] E.W. Lemmon, I.H. Bell, M.L. Huber, M.O. McLinden. REFPROP 10.0: Reference Fluid Thermdynamic and Transport Properties Database. National Institute of Standards and Technology, Boulder, CO, 2018.

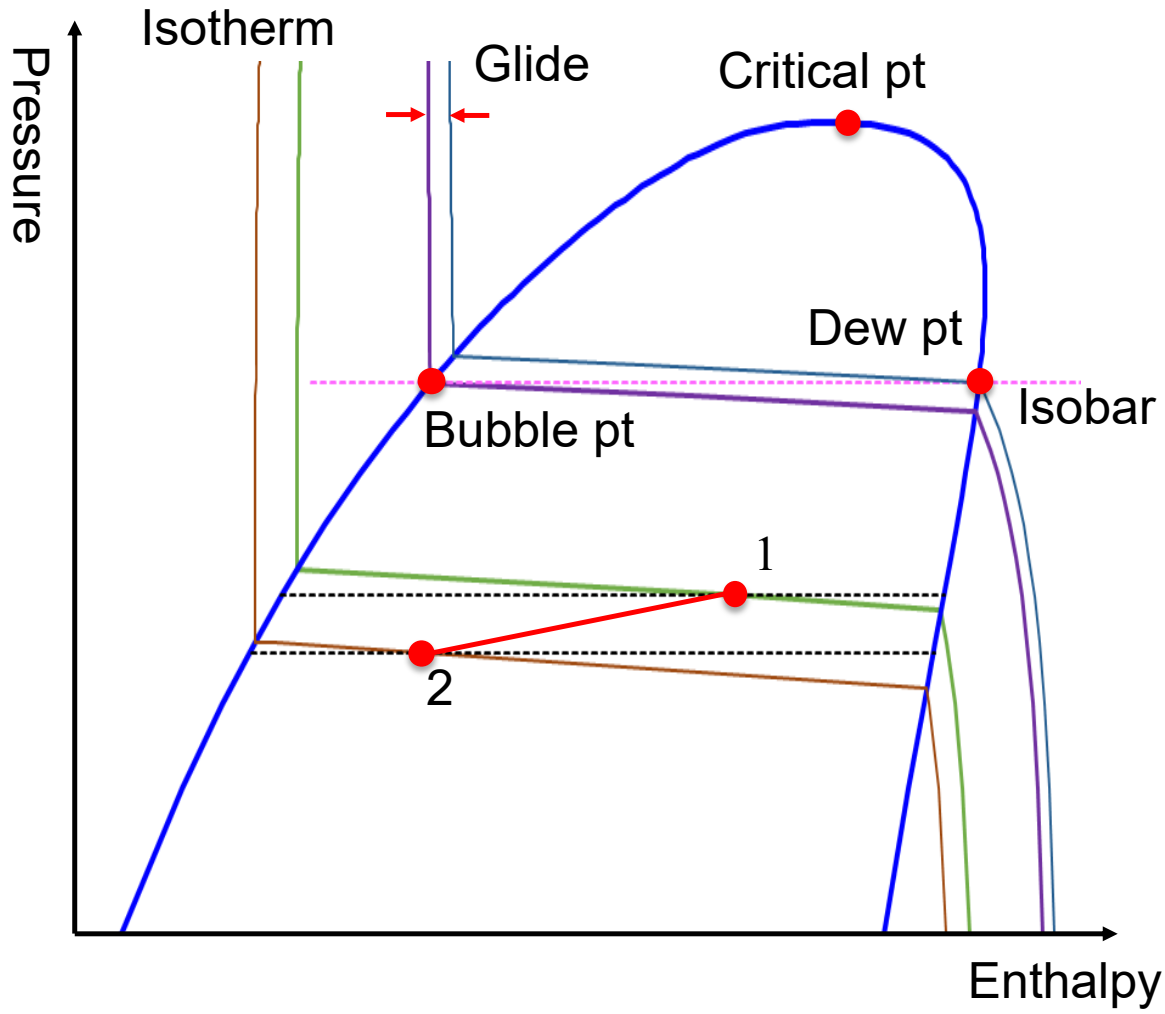

Fig. 1 Temperature glide and pressure drop effects on zeotropic refrigerant phase change

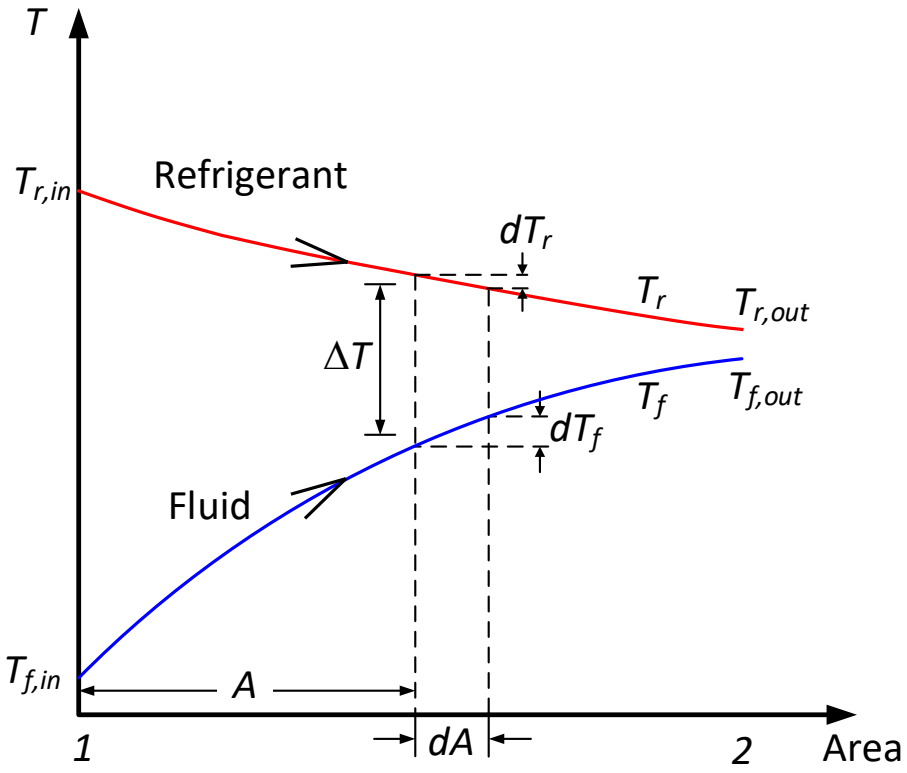

Fig. 2 Temperature profile for a parallel-flow condenser

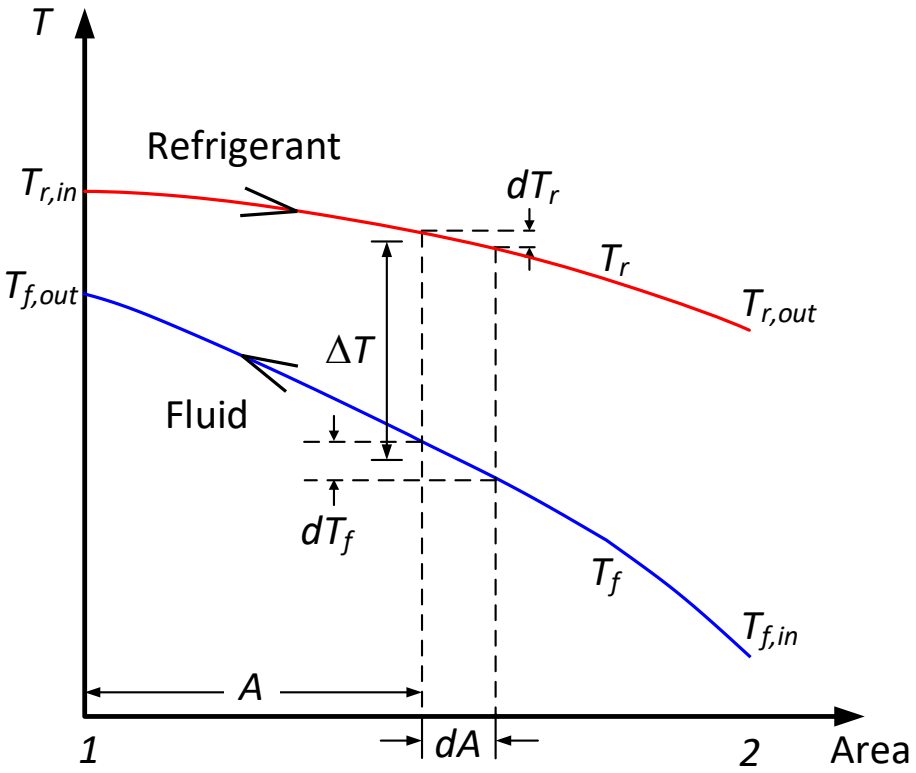

Fig. 3 Temperature profile for a counter-flow condenser

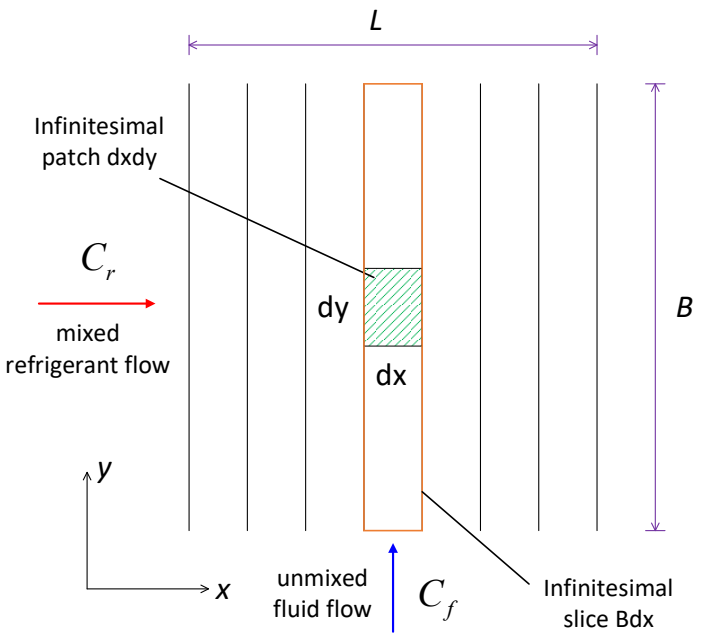

Fig. 4 Cross flow heat exchanger with mixed refrigerant flowing inside a single pipe and unmixed fluid flowing outside between fins

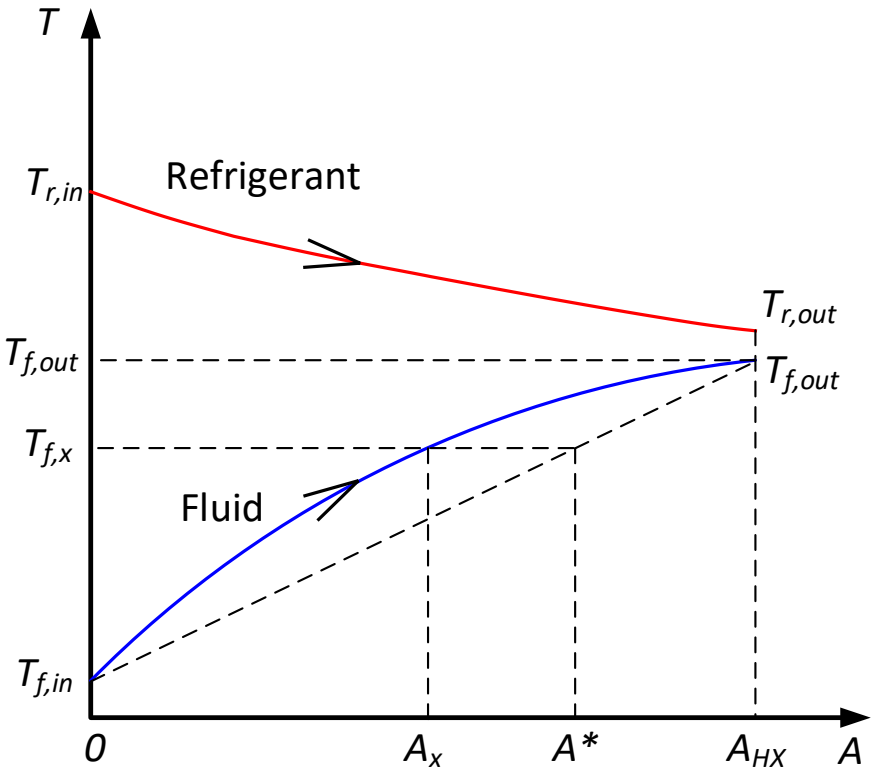

Fig. 5 Curvature of temperature profiles for a parallel-flow condenser

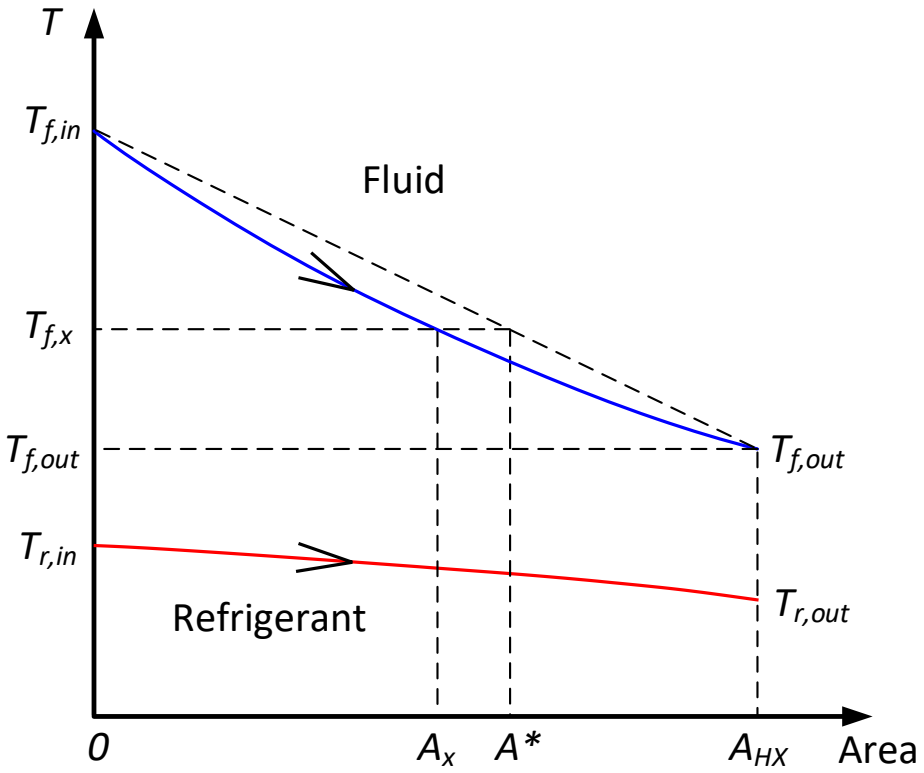

Fig. 6 Curvature of temperature profiles for a parallel-flow evaporator

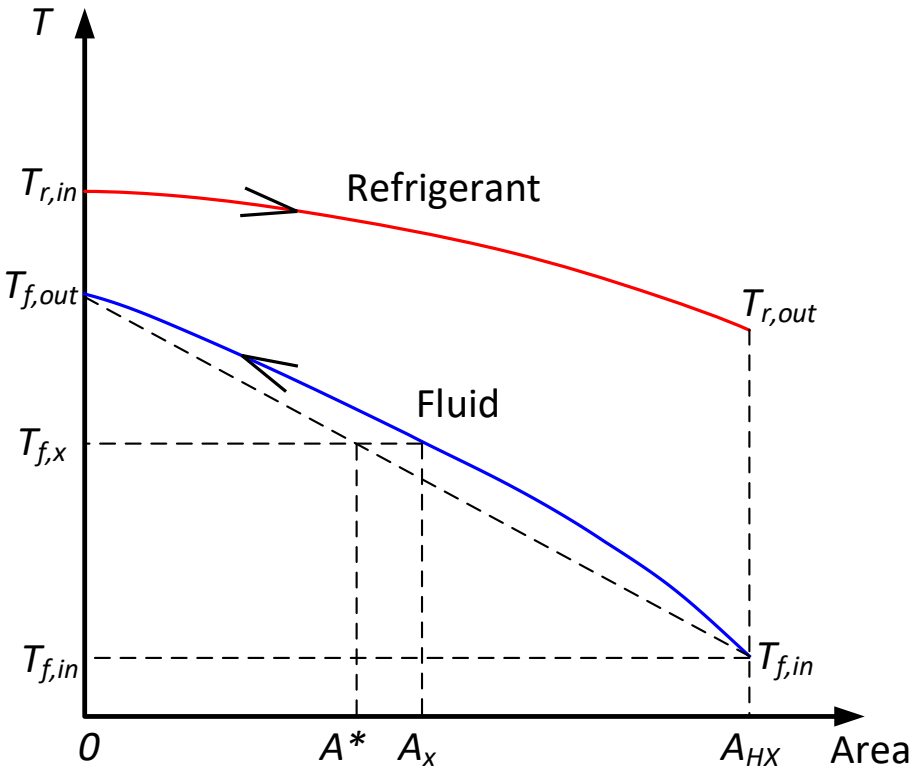

Fig. 7 Curvature of temperature profiles for a counter-flow condenser

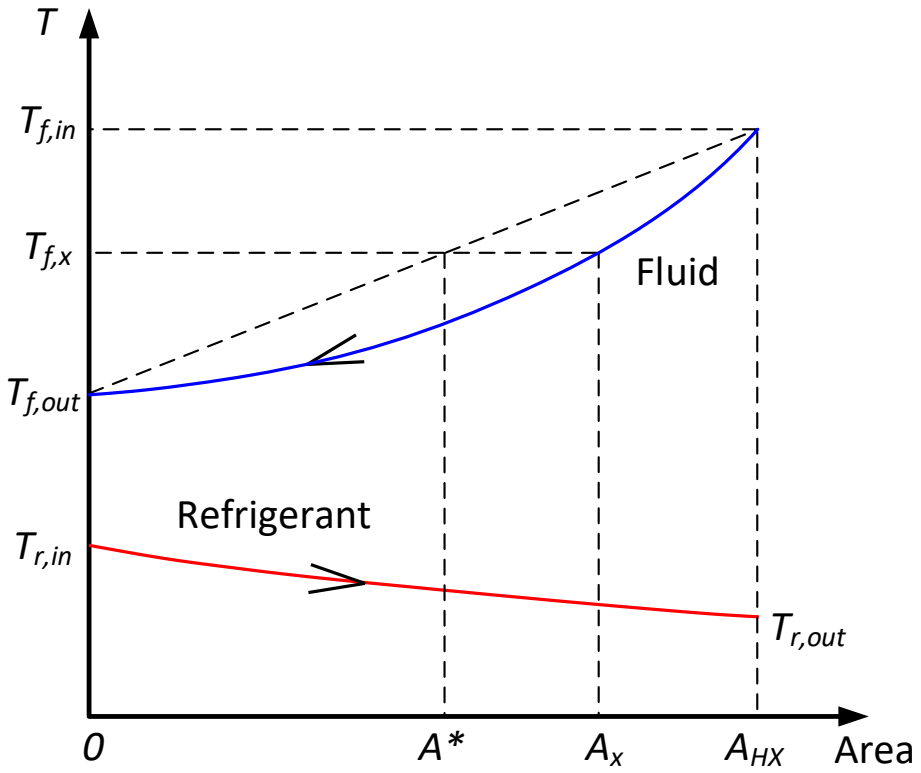

Fig. 8 Curvature of temperature profiles for a counter-flow evaporator

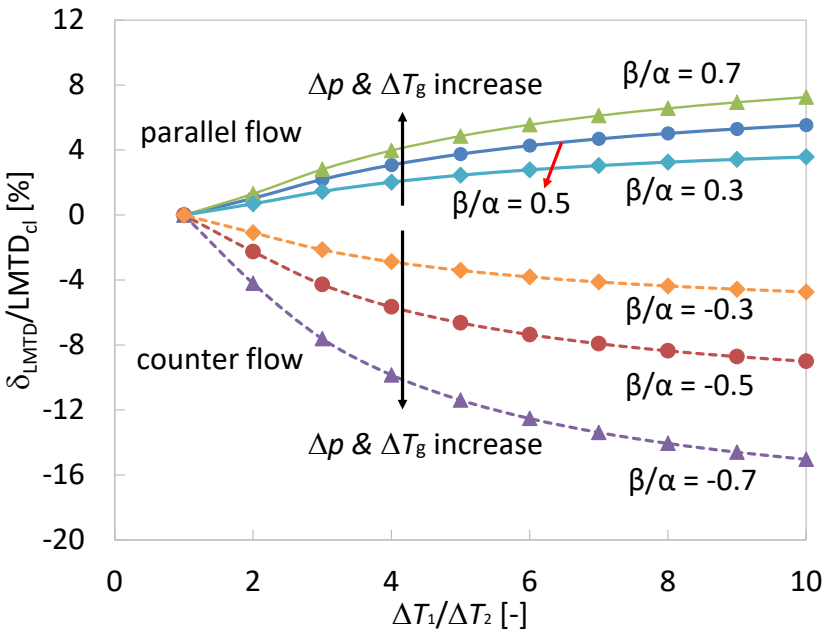

Fig. 9 Relative error between the modified and classical LMTD

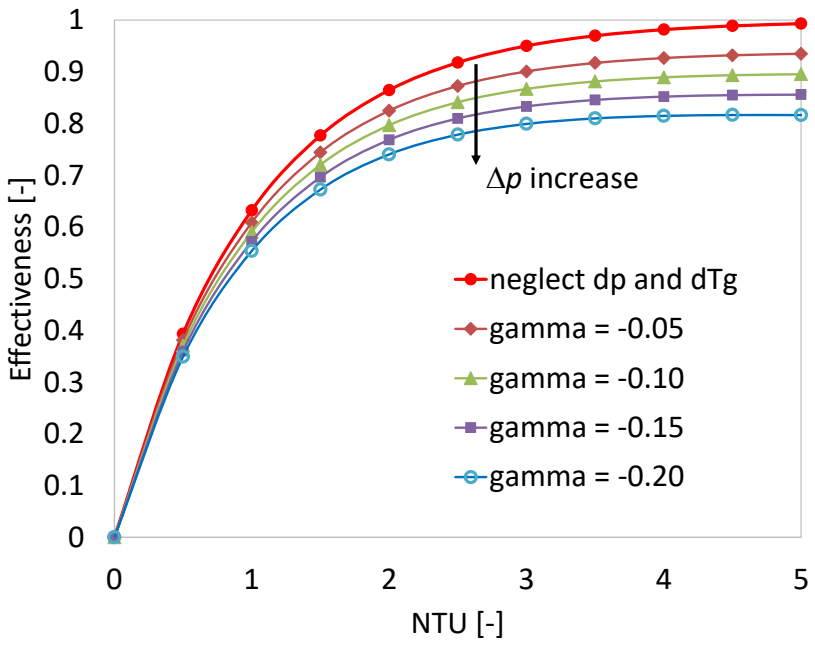

Fig. 10 Effectiveness of a parallel-flow condenser with $\phi = 0.02$

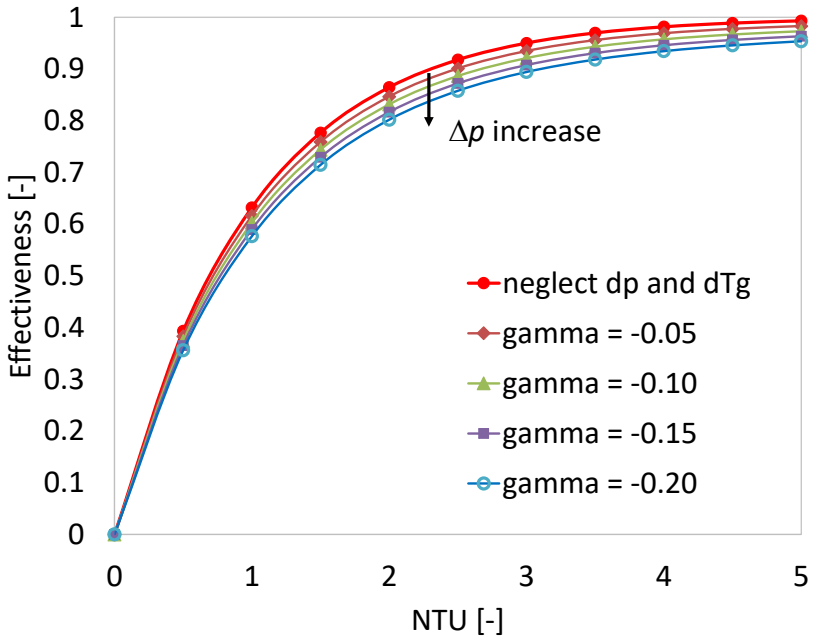

Fig. 11 Effectiveness of a counter-flow condenser with $\phi = 0.02$

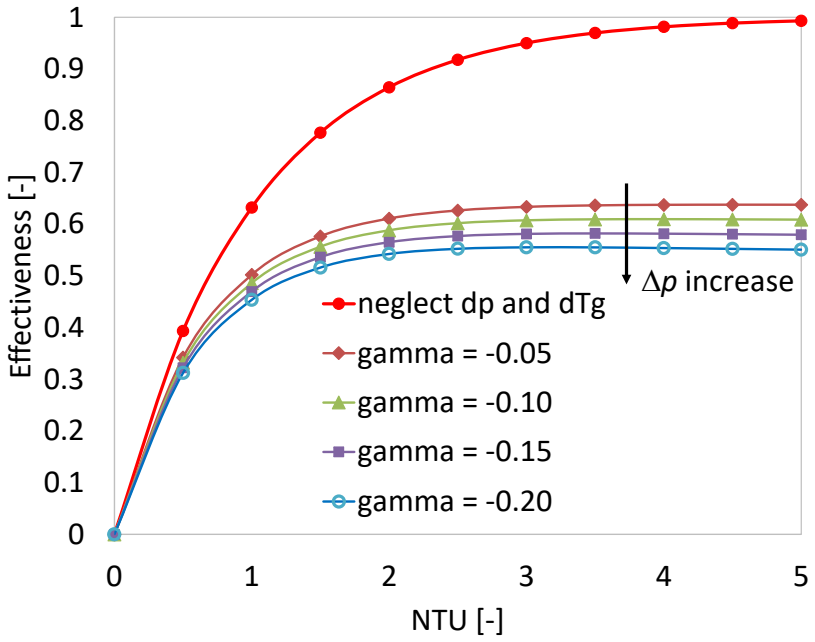

Fig. 12 Effectiveness for a parallel-flow condenser with $\phi = 0.5$

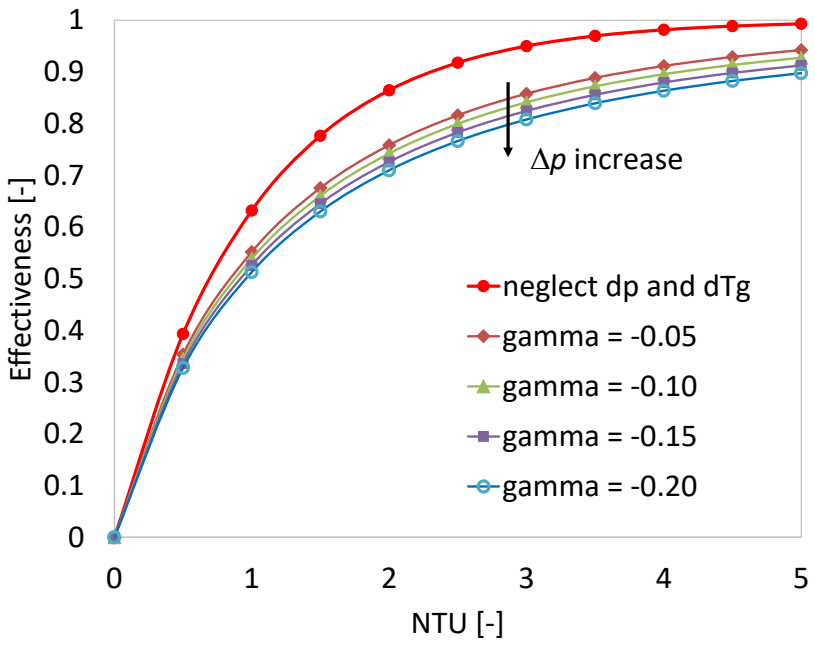

Fig. 13 Effectiveness for a counter-flow condenser with $\phi = 0.5$

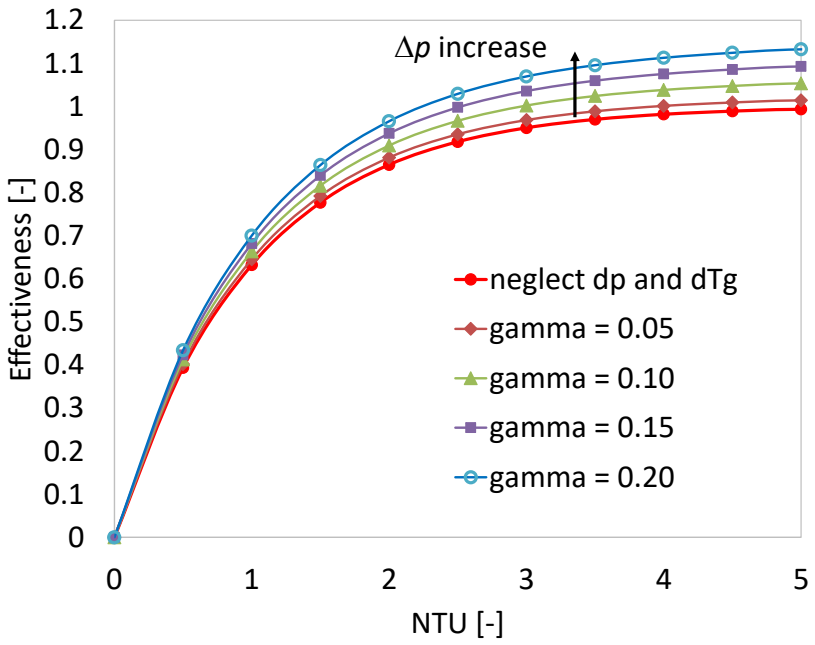

Fig. 14 Effectiveness for a parallel-flow evaporator with $\phi = 0.02$

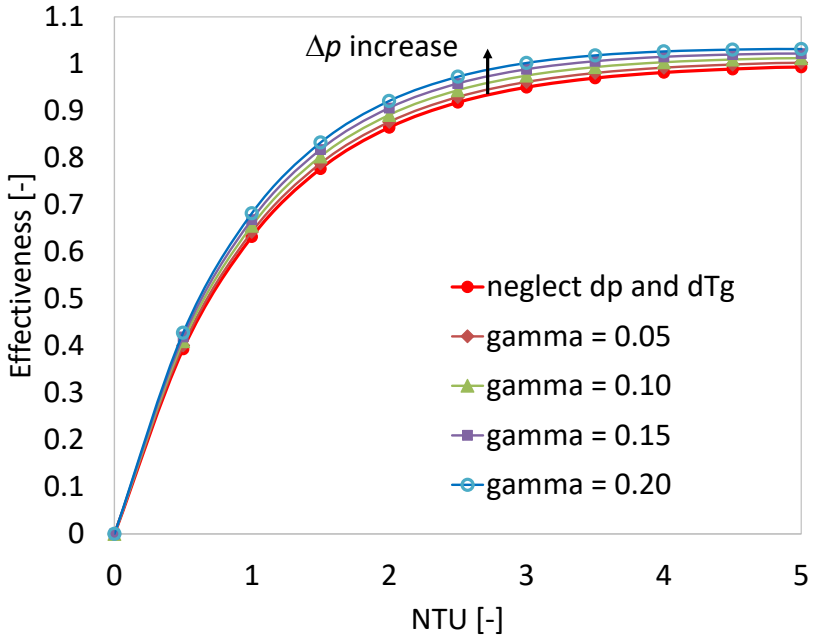

Fig. 15 Effectiveness for a counter-flow evaporator with ϕ = 0.02

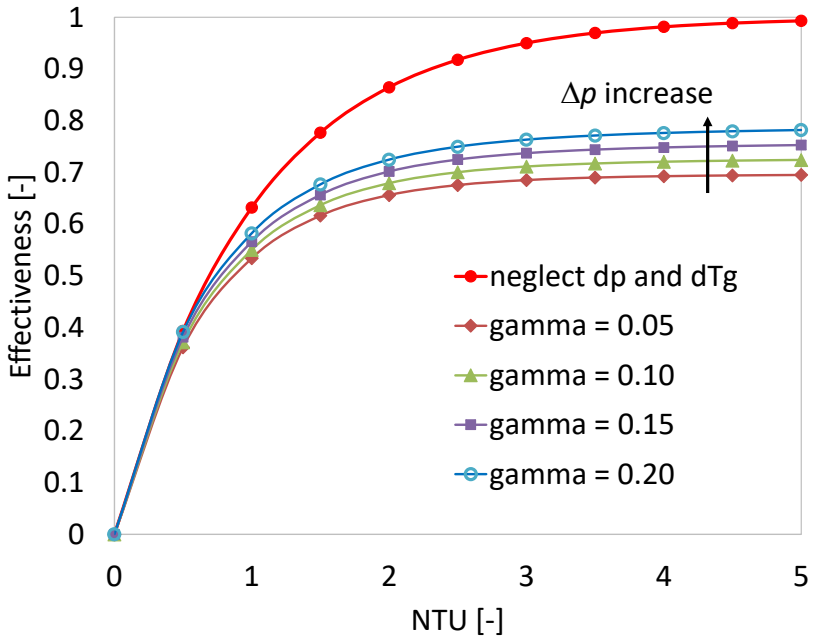

Fig. 16 Effectiveness for a parallel-flow evaporator with ϕ = 0.5

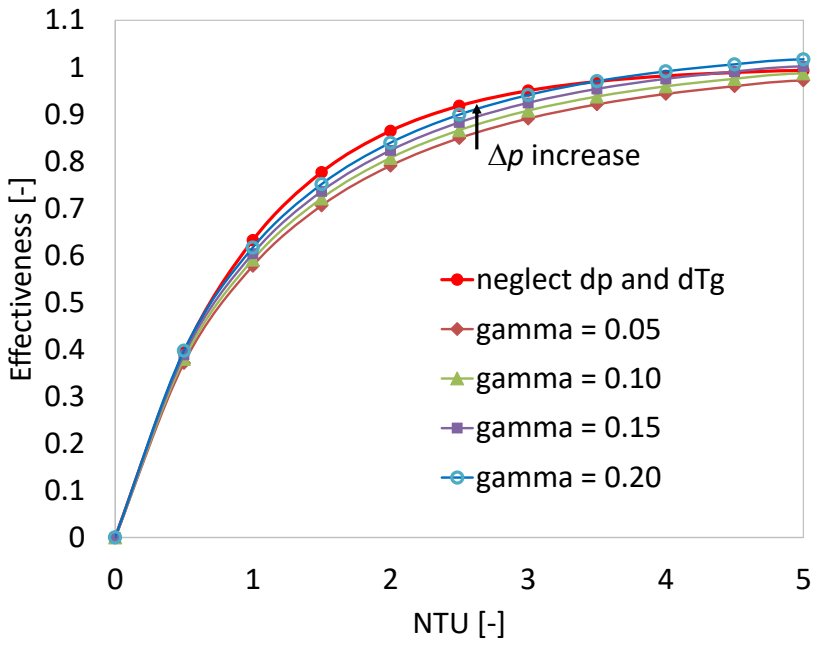

Fig. 17 Effectiveness for a counter-flow evaporator with ϕ = 0.5

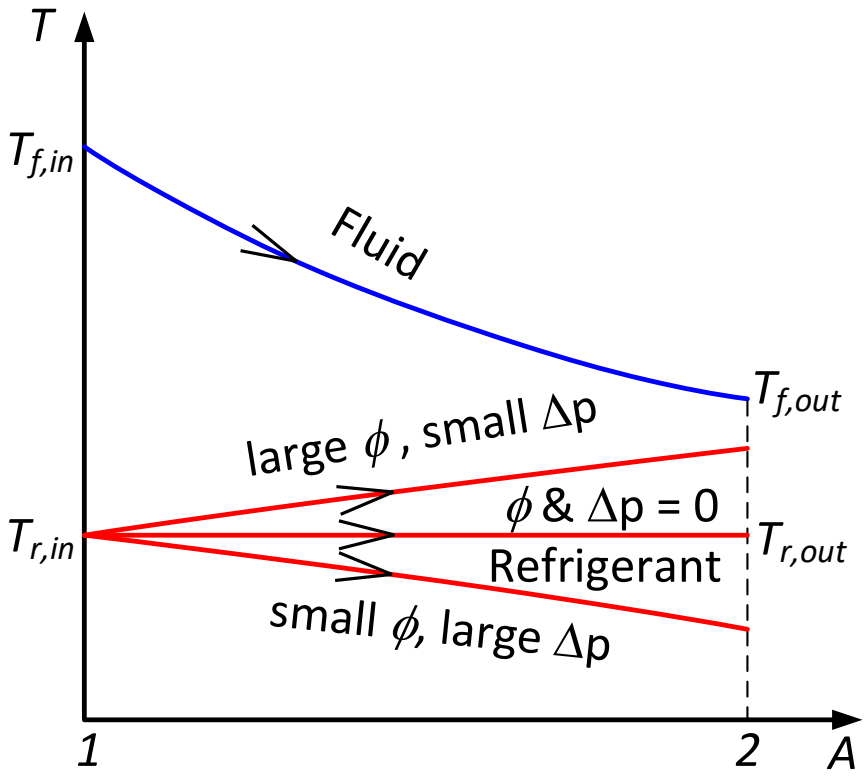

Fig. 18 Temperature profiles in a parallel-flow evaporator showing the effect of pressure drop and capacitance ratio

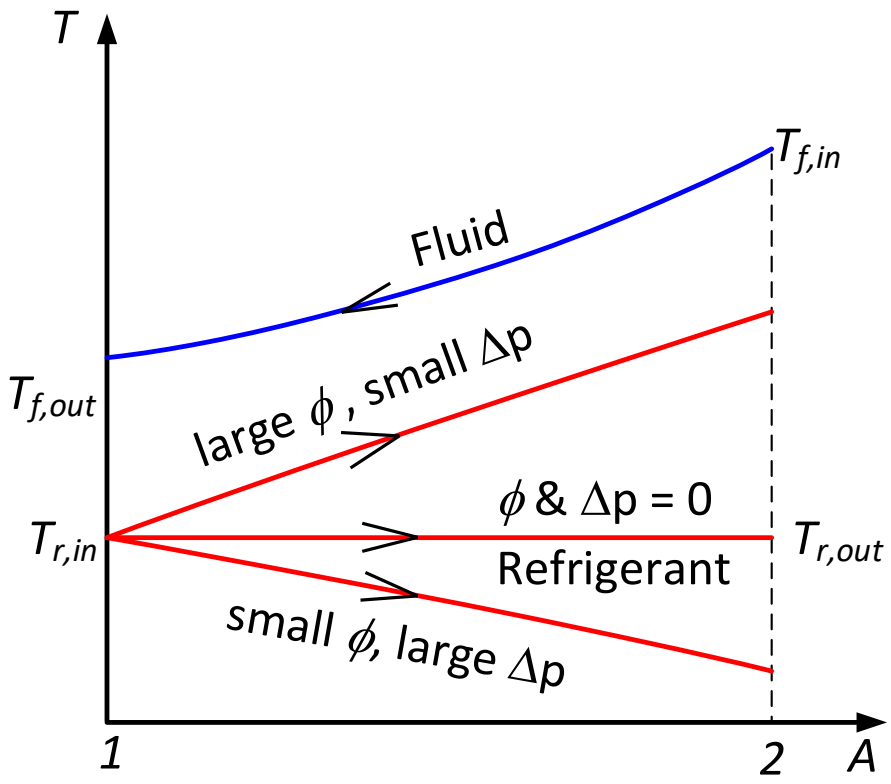

Fig. 19 Temperature profiles in a counter-flow evaporator showing the effect of pressure drop and capacitance ratio

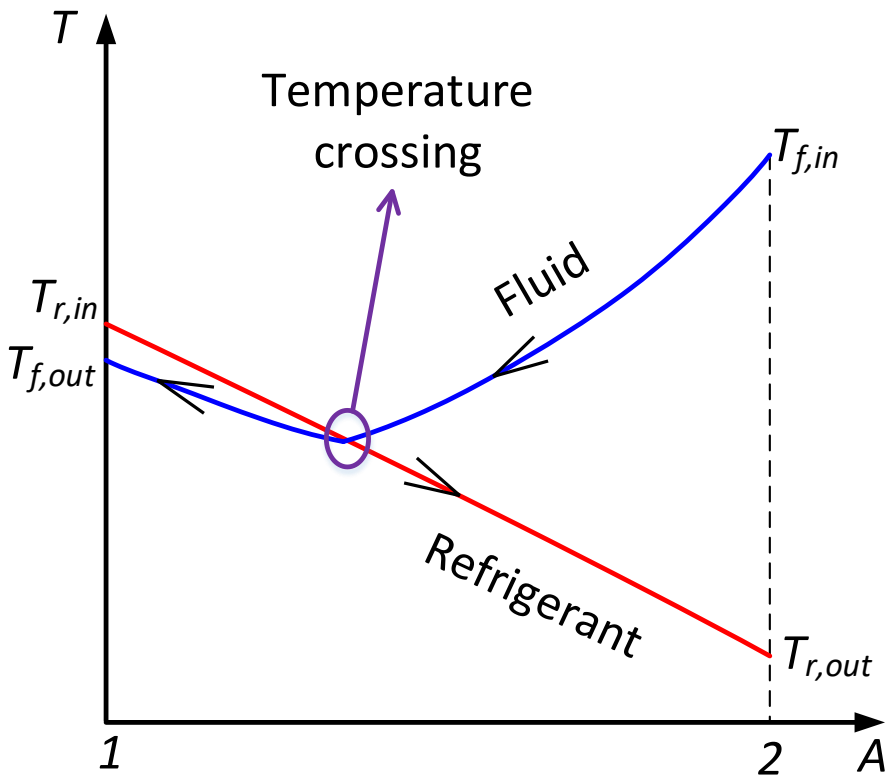

Fig. 20 Temperature profiles in a counter-flow evaporator showing temperature crossing

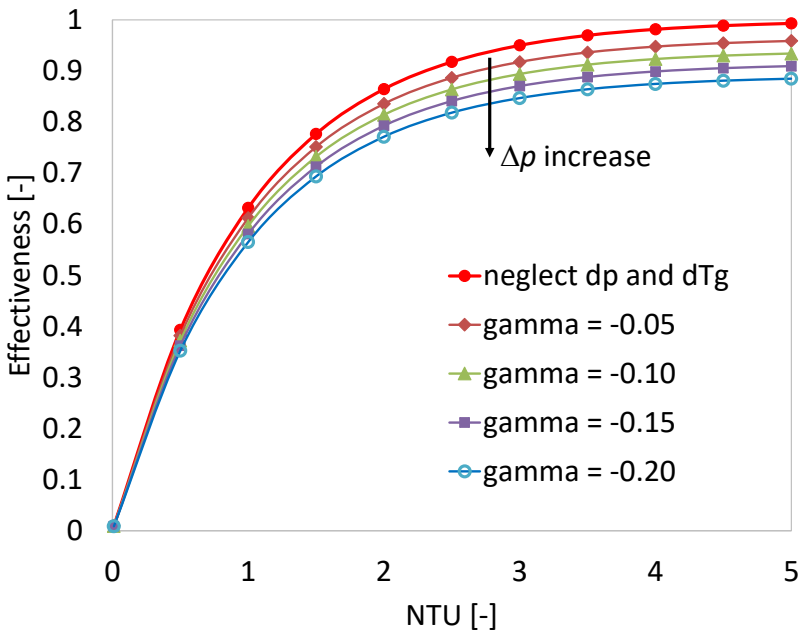

Fig. 21 Effectiveness for a cross-flow condenser with ϕ = 0.02

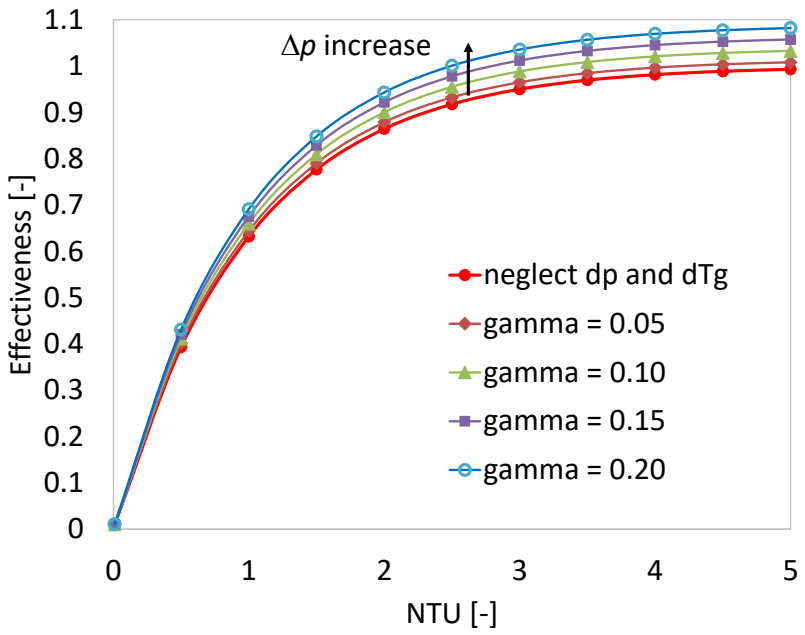

Fig. 22 Effectiveness for a cross-flow evaporator with $\phi = 0.02$

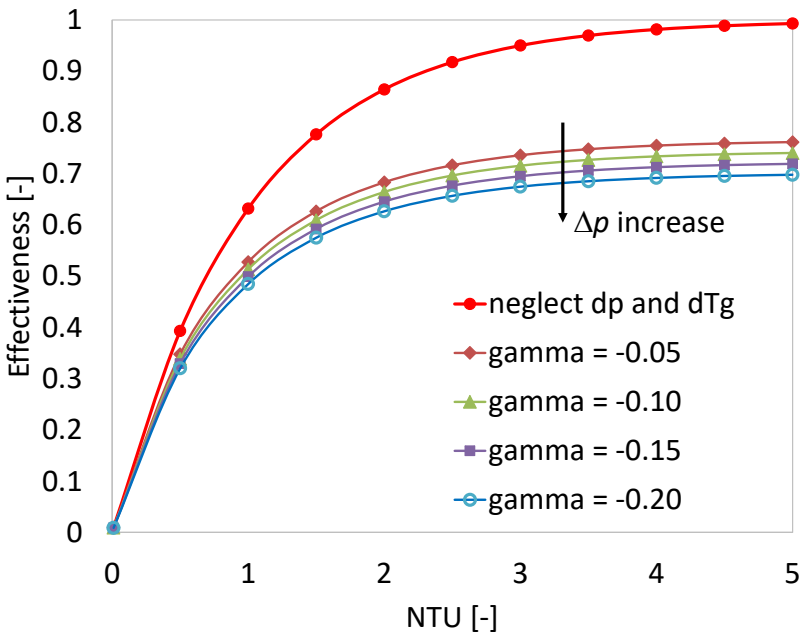

Fig. 23 Effectiveness for a cross-flow condenser with $\phi = 0.5$

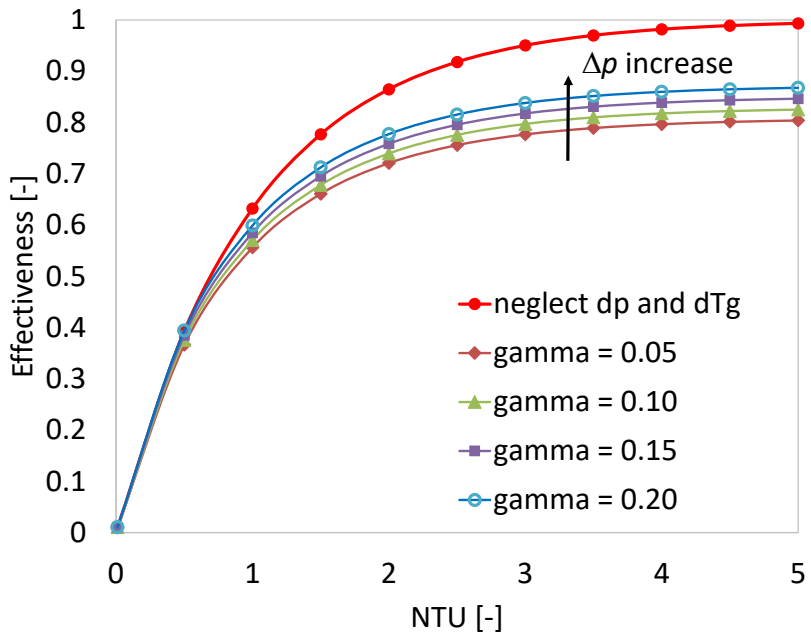

Fig. 24 Effectiveness for a cross-flow evaporator with $\phi = 0.5$

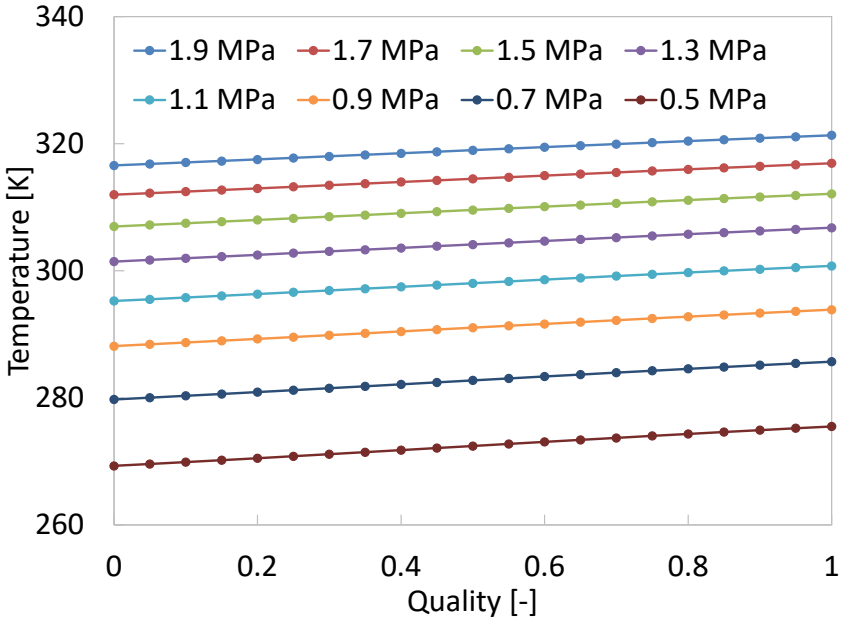

Fig. 25 Two-phase temperature variation of R-407C as a function of vapor quality at different pressures

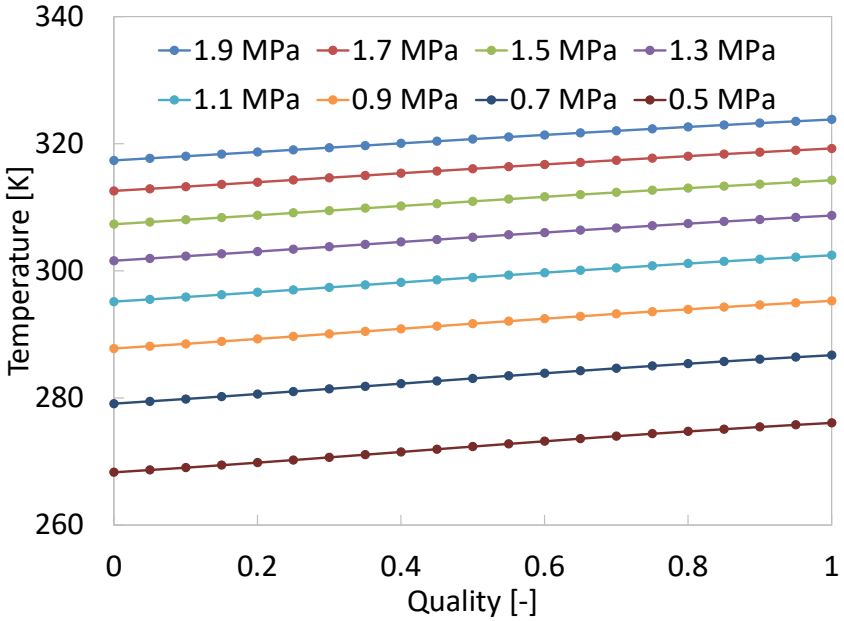

Fig. 26 Two-phase temperature variation of R-454C as a function of vapor quality at different pressures

Table 1. Curvature of Temperature Profiles under Different Flow Arrangements

Flow Type	Process	T_r Profile	T_f Profile
Parallel flow	Condensation	Convex	Opposite to T_r
	Evaporation	Concave if $\Delta p = 0$; otherwise depend on ΔT and ΔT_{sat}	Opposite to T_r
Counter flow	Condensation	$\phi \geq 1$: Convex; $\phi < 1$ (most common): Concave if $\Delta p = 0$; otherwise depend on ΔT and ΔT_{sat}	Same as T_r
	Evaporation	$\phi \leq 1$ (most common): Convex $\phi > 1$: Concave if $\Delta p = 0$; otherwise depend on ΔT and ΔT_{sat}	Same as T_r

Table 2. Relative error trends between corrected and standard LMTD in cross-flow heat exchangers

Condition	Effect on correction term	LMTD error trend	Explanation
$\phi << 1$, low NTU	Very large (denominator << 1)	High error	Both glide and pressure drop correction magnified due to small denominator
$\phi << 1$, high NTU	Moderate to large	Moderate to high error	Glide dominates; pressure drop adds further deviation
$\phi \sim 1$, any NTU	Moderate to small	Low to moderate error	Temperature glide and pressure drop are balanced by fluid-side capacity
$\phi >> 1$, any NTU	Negligible (fluid dominates heat transfer)	Minimal or negligible error	Refrigerant-side variations have little influence on LMTD